# Spatial molecular profiling of mixed invasive ductal-lobular breast cancers reveals heterogeneity in intrinsic molecular subtypes, oncogenic signatures, and mutations

Osama Shiraz Shah[1,3], Azadeh Nasrazadani[1,4], Julia Foldi[7], Jennifer M. Atkinson[1,2], Celina G Kleer[8], Priscilla F. McAuliffe[1,6,] Tyler J Johnston[10], Wayne Stallaert[10], Edaise M da Silva[9], Pier Selenica[9], Higinio Dopeso[9], Fresia Pareja[9], Diana Mandelker[9], Britta Weigelt[9], Jorge S. Reis-Filho[9$], Rohit Bhargava[4], Peter C. Lucas[5], Adrian V. Lee*[1,2], Steffi Oesterreich*[1,2]

[1]Womens Cancer Research Center at UPMC Hillman Cancer Center and Magee Women's Research Institute, Pittsburgh, PA.

[2]Department of Pharmacology & Chemical Biology, University of Pittsburgh, Pittsburgh, PA.

[3]Integrative Systems Biology Program, University of Pittsburgh, Pittsburgh PA.

[4]Department of Pathology, University of Pittsburgh School of Medicine, Pittsburgh, PA

[5]Department of Laboratory Medicine and Pathology, Mayo Clinic College of Medicine and Science

[6]Division of Surgical Oncology, Department of Surgery, University of Pittsburgh School of Medicine, Pittsburgh, PA

[7]Division of Hematology-Oncology, Department of Medicine, University of Pittsburgh, Pittsburgh, PA.

[8]Department of Pathology and Rogel Cancer Center, University of Michigan Ann Arbor, MI 48109, USA

[9]Department of Pathology and Laboratory Medicine, Memorial Sloan Kettering Cancer Center (MSKCC), New York, NY, USA

[10]Department of Computational and Systems Biology, University of Pittsburgh School of Medicine, Pittsburgh, PA

[$]Current affiliation: AstraZeneca

**Keywords:** Mixed invasive ductal and lobular carcinoma, mDLC, digital spatial profiling, DSP, breast cancer, tumor heterogeneity, multi-omics, precision medicine

* Steffi Oesterreich and Adrian Lee share senior authorship

**Corresponding Authors:** Steffi Oesterreich, University of Pittsburgh, 5051 Centre Ave, Pittsburgh, PA 15213. Phone: 412-641-8555, Fax: 412-641-7724, E-mail: oesterreichs@upmc.edu. Adrian Lee, University of Pittsburgh, 5051 Centre Ave, Pittsburgh, PA 15213. E-mail: leeav@upmc.edu.

## Abstract

Mixed invasive ductal and lobular carcinoma (MDLC) is a rare histologic subtype of breast cancer displaying both E-cadherin positive ductal and E-cadherin negative lobular morphologies within the same tumor, posing challenges with regard to anticipated clinical management. It remains unclear whether these distinct morphologies also have distinct biology and risk of recurrence. Our spatially-resolved transcriptomic, genomic, and single-cell profiling revealed clinically significant differences between ductal and lobular tumor regions including distinct intrinsic subtype heterogeneity (e.g., MDLC with TNBC/basal ductal and ER+/luminal lobular regions), distinct enrichment of senescence/dormancy and oncogenic (ER and MYC) signatures, genetic and epigenetic *CDH1* inactivation in lobular, but not ductal regions, and single-cell ductal and lobular sub-populations with unique oncogenic signatures further highlighting intra-regional heterogeneity. Altogether, we demonstrated that the intra-tumoral morphological/histological heterogeneity within MDLC is underpinned by intrinsic subtype and oncogenic heterogeneity which may result in prognostic uncertainty and therapeutic dilemma.

## Significance

MDLC displays both ductal and lobular tumor regions. Our multi-omic profiling approach revealed that these morphologically distinct tumor regions harbor distinct intrinsic subtypes and oncogenic features that may cause prognostic uncertainty and therapeutic dilemma. Thus histopathological/molecular profiling of individual tumor regions may guide clinical decision making and benefit patients with MDLC, particularly in the advanced setting where there is increased reliance on next generation sequencing.

## Main Text

### Introduction

Breast cancer is a prevalent disease worldwide[1] and is the most frequently diagnosed cancer in women in the US, with approximately 300,000 cases per year[2]. The majority (approximately 75%) of cases are classified histologically as invasive breast carcinoma of no special type (IBC-NST), previously described as invasive ductal cancer (IDC). Invasive lobular carcinoma (ILC) is the most common special type accounting for approximately 10-15% of all invasive breast cancer diagnoses[3,4]. Apart from the well-defined histologic and tissue histological differences, there are numerous notable molecular distinctions between ILC and IBC-NST. ILC exhibits enrichment of *CDH1*, *FOXA1*, *TBX3*, *ERBB2* and *PTEN* alterations, while IBC-NST shows a higher frequency of *GATA3*, *MAP3K1*, *TP53* and *MYC* alterations[5]. As a result of *CDH1* alterations, ILC lacks E-cadherin expression, an important cell adhesion molecule[6], and display cytoplasmic p120 staining while IBC-NST retains membranous expression for both molecules[7]. Clinically, ILC is more common in elderly women, presents as larger tumors and is frequently multicentric and multifocal compared to IBC-NST[8,9]. ILC is usually detected later and leads to higher rates of mastectomy [10–14]. ILC is also associated with more frequent metastases to urogenital and gastrointestinal tracts as well as to serosal surfaces than IBC-NST[15,16]. Despite presenting with markers of favorable prognosis, such as low grade, low proliferation index, estrogen receptor positive and human epidermal growth factor receptor (HER2) low/negative, patients with ILC have a higher rate of late recurrences and worse long-term prognosis than those with IBC-NST[14,17,18]. Given its distinct prognosis and outcome compared to IBC-NST, ILC is increasingly

being recognized as a distinct disease, yet it is still treated similarly to IBC-NST in the clinic due to a lack of specific treatment guidelines[14,19,20]. Ongoing clinical trials focused on patients with ILC may lead to the development of more tailored and effective treatment options in the future[20].

Apart from ILC, there are numerous other special types of breast cancers such as mixed invasive breast carcinoma. This is an elusive group of breast cancers which the World Health Organization (WHO) defines as tumors presenting with areas of 10-90% of special histology (such as ILC) admixed with at least 10% of IBC-NST[21]. Importantly, this current WHO definition of mixed invasive breast cancers MDLC differs considerably from its previous definition i.e., tumors presenting with areas of 10-49% of the special subtype and at least 50% IBC-NST[22], indicating the fluid interpretation of this disease. Mixed tumors comprising of both ILC and IBC-NST are the most common (~5-10% of all breast cancer cases[23–28]) and have different terminologies in the literature including mixed invasive ductal and lobular breast carcinoma (MDLC)[29] (used throughout this study), mixed invasive ductolobular breast cancer (MIDLC)[30] ), invasive ductolobular carcinomas (IDLC)[31], and more. Despite increasing appreciation of MDLC disease[32,33], it remains understudied, leading to diagnostic and prognostic uncertainty and clinical management challenges for the patients with this elusive disease. Although there are limited reports focused on MDLC, a few seminal studies have provided insights into its complex pathobiology. Immunohistochemical (IHC) studies have confirmed while that ductal regions of MDLC retain membranous E-cadherin, while lobular regions either lose or display aberrant E-cadherin IHC staining[34–36]. Notably, the current MDLC diagnosis guidelines from WHO only

consider the presence of mixed histological patterns and lack recommendations for support from E-cadherin IHC. However, a recent study suggests that the use of E-cadherin IHC can improve diagnostic accuracy of lobular tumor components in ILC and MDLC tumors[37]. Clinical studies have often yielded contradictory findings[24–26,33,34,36,38,39], but overall, they suggest that MDLC is clinically more similar to pure ILC than IBC-NST[29,40,41 29,40]. These discrepancies may be due to the non-standardized and fluid definition of MDLC disease, limited consideration of its underlying tumor regions and their distinct features and proportions, and the vast intratumoral heterogeneity of this disease[29,33,42,43]. Findings from previous reports point to several subtypes of MDLC tumors based on their histological and E-cadherin staining patterns: 1) intermixed/intermingled type where the E-cadherin positive ductal and E-cadherin negative/aberrant lobular tumor cells appear closely intermixed/intermingled together[31,44], 2) collision type where the E-cadherin positive ductal and E-cadherin negative/aberrant lobular tumor regions appear in spatially distinct regions which may collide into each other forming intermixed regions[31,45], and 3) lobular-like IBC-NST type where there are histologically distinct ductal and lobular tumor regions but the overall tumor is predominately E-cadherin positive[46].

Moreover, molecular studies with profiling of individual tumor regions have been limited. The largest molecular study on MDLC tumors was from the TCGA group[47], where 88 MDLC were classified into lobular-like and ductal-like groups based on transcriptomic and mutational similarity to ILC and IBC-NST tumors. The lobular-like group comprised of ~25% of MDLC cases and showed enrichment of mutations in and lower expression of *CDH1* gene. However, these findings may not have any biological relevance as these samples lacked comprehensive

annotation and may have been incorrectly defined as MDLC as well as the study lacked individual tumor region analysis. Additional molecular studies have largely focused on analysis of somatic genetic alterations[44,45,48]. While these have provided valuable insights into the tumorigenesis pathways and distinct mutational landscape of ductal and lobular tumor regions[36,49], comprehensive studies delineating transcriptomic differences between these distinct regions have not been performed.

To fill this knowledge gap, we employed spatially resolved transcriptomic, genomic, and single cell profiling approaches to comprehensively investigate MDLC and highlight its intratumoral heterogeneity and complexity. We delineate the biological and intrinsic subtype differences between its underlying ductal and lobular tumor regions. Notably, our findings highlight that in some MDLC cases distinct tumor regions with distinct biology may pose distinct progression risk. Hence histopathological and molecular profiling MDLC and its individual tumor regions may inform treatment decisions.

## Results

### Patient Specimens and Their Clinicopathologic Characteristics

A panel of three molecular pathologists identified invasive breast cancer cases diagnosed as "mixed invasive ductal and lobular carcinoma" and shortlisted three cases for this pilot study. All three cases were reported as estrogen receptor positive (ER+) and HER2 negative/low and their ages ranged from 46-63 years (Fig. 1A, Supplementary Table S1A). Assessment of H&E and E-cadherin/p120 dual staining confirmed that each case exhibited histomorphic features in line with the latest MDLC definition i.e., admix of E-cadherin negative lobular tumor regions with at least 10-90% of E-cadherin positive ductal tumor regions[21] (Supplementary Table S1B). Importantly, overall, these cases exhibited collision of spatially distinct ductal and lobular tumor regions[31,45] along with some regions of intermixing and hence could be broadly defined as MDLC of collision type. These cases were particularly amenable for downstream multi-omic profiling compared to those that exhibited more intermingling or intermixing with close proximity of histologic tumor regions. Clinical diagnostic and treatment timelines of these cases, source of their tumor tissue used in this study, and their histomorphic features are illustrated in Fig. 1A. Both MDLC-2 and MDLC-3 eventually developed recurrent disease resulting in patient death in the case of MDLC-2. As of the last follow-up in 2022, in both MDLC-3 and MDLC-1 cases, the patients were alive with tumors, and in the case of MDLC-1 the patient was free of recurrent disease.

### Whole-Transcriptome Spatial Profiling of Ductal and Lobular Regions

152 To better understand the biological heterogeneity and transcriptomic features of ductal and
153 lobular regions, we performed whole-transcriptome digital spatial profiling (DSP) of these three
154 MDLC cases. In total, we analyzed 26 regions of interest (ROIs) with at least 6 ROIs per case.
155 Selected ROIs from a representative case (MDLC-3) are shown in Fig. 1B. We segmented ductal
156 and lobular areas using E-cadherin and Pan-CK staining (Fig. 1C). This enabled profiling of pure
157 ductal and lobular areas from heterogeneous regions that were predominantly of one histology
158 or a mixture of both (Fig. 1D). E-cadherin expression in segmented ductal and lobular regions
159 showed expected results (Fig. 1E). All profiled regions had high RNA sequencing saturation (>
160 94%) and low noise (Q3 count > Negative probe count). However, three regions had low read
161 count (< 0.3 million) and were excluded from further analysis (Supplementary Fig. S1A-C). Our
162 final DSP dataset is comprised of 13 ductal and 13 lobular regions.

163 **Transcriptomic Clusters, Intrinsic Molecular Subtypes and Differential Transcriptomic**
164 **Features**

165 Exploration using top variable genes revealed that regions from each tumor clustered based
166 upon their histology (Fig. 2A; Supplementary Fig. S1D). MDLC-3 ductal regions showed the most
167 distinct mRNA expression compared to all other regions. PAM50 analysis showed both inter and
168 intra-tumor heterogeneity of prognostically relevant intrinsic molecular subtypes (IMS). MDLC-
169 2 ductal regions were a mix of Luminal A and HER2-Enriched subtypes while lobular regions
170 were HER2-Enriched (but stained negative for HER2 IHC – Supplementary Table S1A). MDLC-1
171 ductal and lobular regions were both of luminal IMS, with the former being Luminal A and the
172 latter being Luminal B. Finally, in line with mRNA expression patterns, MDLC-3 ductal and

173 lobular regions showed stark IMS differences (former Luminal A and later Basal-Like). MDLC-3
174 ductal region was the only TNBC/Basal-Like tumor (and had low *ESR1*, *PGR* and *ERBB2* mRNA
175 expression – Supplementary Fig. S1E). We further confirmed the TNBC status of MDLC-3 ductal
176 regions using ER and HER2 IHC (Supplementary Table S1A). Overall, our transcriptomic
177 clustering and IMS analysis suggest that ductal and lobular tumor regions within MDLC may
178 have distinct transcriptomes and intrinsic subtypes.

179 To investigate global transcriptomic differences between ductal and lobular regions across all
180 cases, we performed differential gene expression analysis in a pan-patient manner. To avoid
181 biases caused by fundamental differences between ER+ and ER- disease, we excluded MDLC-3
182 ER-/TNBC ductal regions from this analysis and later downstream analyses (Supplementary Fig.
183 S2C, Supplementary Table S5). In total, we identified 168 significantly up-regulated and 198
184 significantly down-regulated differentially expressed genes (DEGs) in the lobular compared to
185 ductal regions across all cases (Fig. 2B, Supplementary Table S5). These pan-patient DEGs
186 showed strong overlap with patient specific DEGs (Supplementary Fig. S2A-C) indicating that
187 our pan-patient analysis captured most if not all strong global differences between ductal and
188 lobular tumor regions in each case.

189 To assess transcriptomic similarity of MDLC ductal and lobular regions to pure counterparts,
190 i.e., IBC-NST (IDC) and ILC, we compared MDLC ductal vs. lobular region DEGs with those from
191 the comparison of TCGA ER+ IBC-NST (N=327) vs ILC (N=113), respectively (Supplementary Fig
192 S2D). We found *KLK11, KLK10, NRAP, SHROOM1, BTG2,* and *PDK4* were upregulated, while
193 *CDH1*, *DCD, SERPINA1*, and *CPB1* were downregulated in both comparisons (i.e., MDLC ductal vs

194 lobular tumor regions and IBC-NST vs ILC tumors). This overlap confirmed the well-known
195 down-regulation of *CDH1* as a marker of the lobular phenotype as well as potential novel
196 markers.

197 **Differential Enrichment of ER and MYC Signatures & Recurring Biological Themes**

198 To understand the distinct biology of ductal and lobular regions, we scored each DSP region for
199 hallmark signatures[50]. Twenty signatures were differentially enriched between ductal and
200 lobular regions with p-value ≤ 0.05 (Fig. 3A, Supplementary Table S6). Of note, many of these
201 pathways can also be found differentially activated when comparing ER+ IBC-NST and ER+ ILC in
202 TCGA – for example, Kras and TNFA signaling as well as Hypoxia are among significantly
203 enriched pathways in ER+ ILC TCGA samples, whereas Myc targets are enriched in ER+ IBC-NST
204 TCGA samples (Fig. 3B). In line with differential enrichment of Estrogen Response and Myc
205 Target signatures, our transcription factor (TF) signature analysis revealed enrichment of
206 *ESR1/FOXA* TF signatures in lobular and *MYC* TF signatures in ductal regions (Supplementary Fig.
207 S3).

208 To determine recurring biological themes, we expanded our differential enrichment analysis to
209 include all GO[51], REACTOME[52] and KEGG[53] genesets. Signatures differentially enriched between
210 ductal and lobular regions with p-value ≤ 0.05 were further assessed for robustness against
211 background permutations. Robust signatures were grouped into signature clusters based on
212 similarity of overlapping genes in ductal and lobular regions. All signature clusters were further
213 grouped into broad biological themes based on the underlying biological terms (Fig. 3C, left
214 panel). The mean score of all signature clusters in ductal and lobular regions is shown in Fig. 3C,

right panel. Lobular regions were enriched for TP53 & senescence, collagen & extracellular matrix (ECM), MAPK/ERK targets (in line with KRAS signatures shown in Fig. 3A), while ductal regions were enriched in double stranded break & homologous repair (DSB/HR), mTOR signaling (in line with Mtorc1/Mtor signatures shown in Fig. 3A) among other signatures (Supplementary Table S7).

Notably, several genes including *MYC, G3BP1* and *SNRPD1* overlapped between Myc Targets V1 and G2m Checkpoint signatures (both enriched in ductal regions). Both of these signatures had no overlapping genes with DNA damage and repair (D1: DBS/HR) signatures (Supplementary Fig. S4A) indicating that Myc related signatures in ductal regions are associated with proliferation. Importantly, various senescence and cell death related genes (*CDKN1A/2B/2C, TP53, BCL6* among others) overlapped between the L1: Cell cycle and L2: *TP53* & Senescence signatures indicating negative regulation of cell cycle via *TP53* signaling and cell cycle inhibitors (Supplementary Fig. S4B). Key genes associated with these notable and other biological signatures are highlighted in Supplementary Fig. S4C. In summary, we identified various differentially enrichment of various oncogenic and biological signatures between ductal vs. lobular regions including cell cycle (Myc and G2m genes in ductal, and TP53 and cell cycle arrest genes in lobular), immune, collagen & ECM and metabolism among others.

To further investigate some of the notable distinctions in gene expression signatures between ductal and lobular tumor regions, we performed multiplexed immunofluorescence to obtain single-cell proteomic measurements of key cell cycle and senescence effectors in ductal and lobular tumor cells, identified by staining for pan-cytokeratin 26 and E-cadherin (Fig. 3D,

236 Supplementary Table S12). Individual cells within ductal regions exhibited significantly higher
237 expression of proliferative markers including cMYC, cyclin E2, and cyclin A1, while lobular
238 regions had significantly higher expression of the senescence biomarker p16 (Fig. 3E). These
239 findings confirmed the activation of Myc signaling and proliferative pathways in ductal, and
240 activation of cell cycle arrest/senescence in lobular tumor regions.

241 **Genomic Landscape and Clinically Relevant Genomic Alterations**

242 To explore the genomic landscape of ductal and lobular regions, we employed the FDA-
243 approved targeted MSK-IMPACT panel. We micro-dissected the ductal and lobular tumor
244 regions from FFPE blocks of each case and sequenced them at a median depth of 416x (range
245 287–563) (Supplementary Fig. S5A). In all cases, at least one pathogenic mutation was detected
246 in known breast cancer driver genes, including *CDH1, PIK3CA, TP53, GATA3, KMT2C, MAPK31,*
247 *ARID1A,* and *CBFB*, in both ductal and lobular regions, as depicted in Fig. 4A. Furthermore, all
248 pathogenic mutations had a high cancer cell fraction (Supplementary Fig. S5B).

249 Loss of E-cadherin is an established driver of lobular tumorigenesis[54]. Typically, it results from
250 biallelic *CDH1* inactivation, through a combination of truncating mutation and loss of
251 heterozygosity (LOH)[28]. All lobular regions exhibited loss of E-cadherin, with both MDLC-1 and
252 MDLC-3 harboring *CDH1* truncating mutations and LOH (Fig. 4B; Fig. 1E; Supplementary Fig.
253 S1E). The lobular region of MDLC-2 did not have *CDH1* genomic alterations but showed
254 epigenetic inactivation via methylation of its promoter. A putative passenger mutation in *CDH1*
255 was also observed in the MDLC-3 ductal region, which had no effect on mRNA or E-cadherin
256 levels (Fig. 1E; Supplementary Fig. S1E). The loss of E-cadherin is consistent with the

257 downstream down-regulation of Adherens Junction signatures in all lobular regions (Fig. 3A).
258 Hotspot *PIK3CA* mutations, which are early oncogenic driver events frequently observed in ER+
259 BC[55], were present in all cases except MDLC-3. The MDLC-1 ductal region had mutations in
260 *GATA3* (critical transcriptional binding partner of ERalpha[56]) and *CBFB* (forms complex with
261 *RUNX1* to suppress NOTCH signaling[57]). The MDLC-3 ductal region had loss of *TP53*, an event
262 associated with more aggressive types of breast cancer like basal/TNBC[58] and consistent with its
263 basal-like intrinsic subtype. MDLC-2 ductal region had truncating mutation in *KMT2C*, an
264 important regulator of ER alpha activity[59]. MDLC-3 lobular region had mutations in *ATRX* and
265 *ARID1A,* two chromatin remodeling and DNA repair genes[60]. In addition, while MDLC-1 and
266 MDLC-3 ductal and lobular regions did not share any somatic clonal mutations, MDLC-2 ductal
267 and lobular regions shared several somatic clonal mutations in *PIK3CA* and *MAPK31* genes
268 indicating shared tumor origin.

269 To investigate the copy number (CN) landscape of ductal and lobular regions, we performed CN
270 analysis using FACETS[61] (Fig. 4B). All regions exhibited breast cancer characteristic chromosome
271 1q gains and 16q losses[58]. Overall, ductal tumor regions showed more frequent aneuploidy
272 events than lobular tumor regions. MDLC-3 ductal region showed the most aberrant CN profile
273 consistent with its basal/TNBC etiology[58]. Moreover, chromosome 22 aneuploidy was only
274 observed in ductal tumor regions. Notably, both histologic regions of MDLC-3 and ductal region
275 of MDLC-2 had *NOTCH2* gains or amplifications (Supplementary Fig. S5C).

276 **Mutational Processes Driving Tumor Evolution**

To determine the mutational processes underlying the evolution of ductal and lobular tumor regions within MDLC, we performed mutational signature analysis of all cases (Fig. 4C). Both histologic regions in MDLC-2 were associated with an "aging" signature. In MDLC-3, ductal region was associated with homologous repair deficiency (HRD) while the lobular regions with APOBEC signature. Tumors with an APOBEC signatures have a higher frequency of mutations in chromatin remodeling and DNA repair genes[62], as seen in MDLC-3 lobular region. We did not identify any signatures for MDLC-1 ductal and lobular regions. The putative evolution of each MDLC case and its histologic region based upon the mutations, *CDH1* alterations and mutational signatures is shown in Fig. 4D. Notably, the MDLC-2 ductal and lobular regions not only shared clonal pathogenic (*PIK3CA*) and passenger (*MST1R* and *MAP3K1*) mutations but also the "aging" mutational signature. Loss of function *CDH1* alterations were hallmark of all lobular regions across cases.

**Single-Cell RNA-Sequencing and Identification of Ductal and Lobular Populations**

To explore the heterogeneity of MDLC at a single-cell level, we performed scRNAseq sequencing of a fresh tumor specimen from MDLC-1. The resulting scRNAseq comprised of 4,671 cells and had sequencing saturation, reads in cell and median genes per cell as shown in Supplementary Fig. S6A. Cell-type annotation based on canonical markers (see details in Supplementary Methods) revealed various tumor and non-tumor cell types (Supplementary Fig. S7B). scRNAseq inferred copy number revealed that only the epithelial tumor cells had aneuploid copy number status further confirming their nature (Supplementary Fig. S7C). For the downstream analyses, we only focused on the tumor cell cluster. Clustering of this revealed two

298 transcriptionally distinct tumor cell populations with similar cell cycle profiles; however, we
299 were unable to annotate them as either ductal or lobular tumors using *CDH1* mRNA expression
300 (Fig. 5A). Notably, while the MDLC-1 lobular regions showed loss of E-cadherin protein (Fig. 1E),
301 the *CDH1* p.Q23* truncating mutation in these regions (Fig. 4A) didn't alter *CDH1* mRNA
302 expression (Supplementary Fig. S1E). Previous studies suggest that some protein truncating
303 mutations can escape non-sense mediated decay and thereby maintain gene expression levels
304 but lack a functional protein[63–65]. Indeed, similar effects of Q23 mutations were seen in the
305 TCGA cohort, where *CDH1* mRNA levels in Q23* mutant tumors were similar to those in *CDH1*
306 WT tumors, while the E-cadherin protein levels in Q23* mutant tumors were similar to the
307 tumors with all other *CDH1* truncating mutations (Supplementary Fig. S6).[63–65]

308 To identify ductal and lobular single populations, we derived ductal and lobular transcriptome
309 signatures (Supplementary Table S5) from differential gene expression analysis of the MDLC-1
310 DSP ductal vs lobular tumor regions and used these signatures to score each single cell in
311 MDLC-1 scRNAseq dataset. Using this deconvolution approach, we successfully annotated
312 ductal and lobular tumor populations in the scRNAseq dataset (Fig. 5B). scRNAseq inferred copy
313 number profiles of ductal and lobular cells revealed various breast cancer specific
314 aberrant/aneuploid events in chromosomes 1, 8, 11, 16, 18 among others (Supplementary Fig.
315 S7E). Overall, the copy number profiles of ductal tumor cells were more aberrant than those of
316 lobular tumor cells. Ductal and lobular tumor regions DEGs in scRNAseq and DSP datasets
317 showed significant overlap (Supplementary Fig. S7D,F). Differential enrichment of several
318 hallmark signatures and recurring biological themes in ductal and lobular regions from DSP data

was recapitulated in our scRNAseq data (Supplementary Fig. S8A,C). Notably, we saw enrichment of Estrogen and senescence signatures in lobular and Myc signature in ductal tumor cells in both DSP and scRNAseq datasets.

**Single-Cell Heterogeneity and Mapping of Single-Cells to Spatial Regions**

To investigate single-cell heterogeneity of ductal and lobular populations, we increased resolution of clustering to identify sub-clusters. Each sub-cluster had unique marker genes (Fig. 5C) and several of these also showed differential enrichment of hallmark signatures and recurring biological theme clusters (Supplementary Fig. S8B,D), indicating intra-tumor heterogeneity within ductal and lobular tumor populations. To investigate whether single-cell transcriptomic heterogeneity was associated with spatial heterogeneity, we mapped scRNAseq sub-clusters to DSP regions. To assess similarity between each region and sub-cluster, we scored all regions for sub-cluster marker genesets using GSVA (Fig. 5D). Each region was mapped to a sub-cluster for which it had most similarity (i.e., highest GSVA score) (Fig. 5E). The top five marker genes of each scRNAseq sub-cluster (Supplementary Fig. S7G) are shown beside each sub-cluster and spatial region link. These findings perhaps suggest that the single-cells in each sub-cluster came from a spatially distinct niche in the tumor.

## Discussion

Despite an increasing incidence of MDLC[32,33], this special subtype of breast cancer remains poorly understood, with limited knowledge about its overall biology and that of its underlying ductal and lobular tumor regions, as well as their clinical implications.

Spatially resolved and single-cell profiling techniques have revolutionized our understanding of physiological and pathological processes and tissue architecture[66]. Efforts such as Human Cell Atlas[67] have successfully uncovered the major cell types and their spatial organization in both normal breast tissue[68,69] and breast cancer[70]. Spatial and single-cell profiling of primary breast cancer subtypes and metastatic disease have been instrumental in identifying novel molecular features and their prognostic value[71–75]. However, to date genome-wide spatial and single-cell investigation of MDLC has not been reported. To address this gap, we employed spatially resolved transcriptomics, genomics, and single-cell profiling to investigate the biology of individual tumor regions within MDLC of collision type. Our study confirmed various previously reported observations of genetic inactivation of *CDH1* and concomitant loss of E-cadherin in lobular regions[31,34–36] and the presence of distinct driver alterations in individual tumor regions[31,36]. We also uncovered novel findings that highlight the vast heterogeneity within MDLC, several of which may be indicative of distinct prognosis, hence highlighting the significance of reporting this heterogeneity in clinical diagnosis. Ductal and lobular tumor regions had distinct biological signatures, in particular cell cycle arrest/senescence, ER and *MYC* signaling, and intrinsic molecular subtypes (IMS). The IMS distinctions were most prominent in the case of MDLC-3, which was clinically reported as ER+ tumor but molecular profiling revealed

356 that the underlying ductal region was ER-/TNBC with basal-like IMS while the lobular region was
357 ER+ with luminal-A IMS. Notably, both ER- status and basal-like IMS are associated with worse
358 prognosis and outcome than ER+ and luminal IMS[76,77]. In this case, the patient had brain and
359 lung metastases, both of which were also ER-, suggesting progression of the primary ER- ductal
360 tumor. Another notable finding was enrichment of cell cycle arrest/senescence and ER signaling
361 signatures in lobular while *MYC* signatures in ductal tumor regions. Multiplex
362 immunofluorescence staining of various effector proteins confirmed that Myc and Cell
363 proliferation signaling were active in ductal tumor cells, while cell cycle arrest/senescence
364 signaling was active in lobular regions. Further analysis at single-cell RNA level revealed that ER
365 signatures were enriched in only one lobular subcluster (L2), highlighting molecular
366 heterogeneity even within individual histologically distinct tumor regions. Majority of ILC are
367 strongly ER+ and respond well to endocrine therapies, while they are mostly less proliferative,
368 responding poorly to chemotherapy[14,20,28,78,79]. Whether this is also true for lobular regions
369 within MDLC is an important question and must be further investigated. Perhaps, future trials
370 can study whether tumors with predominantly ductal vs. lobular MDLC respond differently to
371 endocrine and chemotherapies.

372 Development of robust mutational signature analysis tools such as Signature Multivariate
373 Analysis (SigMa) have allowed accurate identification of mutational signatures associated with
374 such HRD and APOBEC defects from targeted sequencing panels such as MSK-impact[80–84].
375 Utilization of SigMa algorithm in our study revealed that individual tumors regions with distinct
376 alterations may share common (Aging in MDLC-2) or distinct (APOBEC or HRD in MDLC-3)

377 mutational signatures. Collectively, our results indicate ductal and lobular regions in MDLC-2
378 have shared origin, while MDLC-3 is a clear collision of two independent tumors. The etiology of
379 MDLC-1 is questionable – while there are no shared mutations, we note that this interpretation
380 is based upon a small panel of genes measured by the MSK IMPACT panel with strict filtering.
381 We cannot exclude the possibility of shared mutations in other cancer-related genes not
382 covered by MSK-impact panel. Larger efforts using whole genome profiling of more MDLC
383 tumors are needed to comprehensively investigate the mutational signatures and origins of
384 ductal and lobular tumor regions in mixed tumors.

385 The presence of distinct clinically actionable alterations in individual tumor regions within
386 MDLC is of clinical relevance and has been previously reported MDLC[45]. Tumor regions with
387 distinct alterations can complicate clinical management. Alterations in components of ER
388 signaling (such as *GATA3, KMT2C*) as well as Notch signaling (*CBFB*, *NOTCH2*) can lead to
389 endocrine resistance[85–87], while alterations in DNA repair response genes (*ARID1A*, *ATRX*) may
390 confer increased sensitivity to chemotherapy and other DNA repair pathway targeting drugs
391 including PARP inhibitors[88,89]. Future studies will need to address the important question
392 whether treatment decisions for patients with MDLC benefits from considering the distinct
393 alterations in individual tumor regions.

394 For a long time, it was unclear whether ductal and lobular regions within MDLC share any
395 molecular similarity with their pure counterparts (i.e., ILC and IBC-NST tumors). To fill in the
396 gap, in our study, we compared the molecular features of individual tumor regions within MDLC
397 with their pure counterparts (i.e., ILC and IBC-NST tumors) in the TCGA cohort[28] and discovered

398 a set of shared markers of lobular phenotype. There was some but limited overlap of the
399 differentially expressed genes between ductal and lobular tumor regions in MDLC cases with
400 differential gene expression in ER+ ILC vs ER+ IBC-NST in the TCGA cohort. This could be due to
401 technical reasons such as bulk sequencing of frozen tumor samples (in TCGA) vs. spatial
402 sequencing of epithelial tumor regions from FFPE tissues (in this study). Furthermore, this also
403 could also be reflective of true biology i.e., unique gene expression patterns in MDLC tumor
404 regions compared to pure ILC and IBC-NST tumors. As expected, one of overlapping genes that
405 was downregulated in both MDLC lobular tumor regions and ILC tumors was *CDH1*, an
406 important driver of lobular tumorigenesis[54]. [2854]This primarily occurs via genetic inactivation of
407 *CDH1* in ILC tumors[28], similar to what was observed in the case of lobular regions in MDLC-1
408 and MDLC-3. However, in the lobular region of MDLC-2, *CDH1* promoter methylation was
409 observed. *CDH1* promoter methylation is also associated with epithelial-to-mesenchymal
410 transition (EMT), however, EMT is not a typical feature of lobular tumors and is primarily
411 associated more complex subtypes of breast cancers such as metaplastic and claudin-low
412 subtypes[90–93]. EMT markers[90] (Supplementary Fig. S1F) were not consistently upregulated in
413 MDLC-2 lobular region hence ruling out EMT-associated *CDH1* promoter methylation. This is an
414 intriguing observation, suggesting that the pathogenesis of lobular regions within MDLC may
415 occur via both genetic and epigenetic inactivation of *CDH1,* unlike ILC where genetic
416 inactivation of *CDH1* is predominant[6,31,94–96]. A recent study revealed the synthetic lethality in E-
417 cadherin deficient breast cancers with inhibition of *ROS1*, a tyrosine kinase[97], and trials are
418 ongoing testing efficacy of *ROS1* inhibitors in ER+ ILC disease. Future studies could assess *ROS1*

419 inhibitors or other drugs in treating patients with predominantly lobular MDLC disease.
420 Additional studies are also warranted to investigate whether E-cadherin deficient tumors with
421 distinct etiology, such as *CDH1* epigenetic inactivation, have distinct biology potentially
422 associated with differential treatment response.

423 Our study focused primarily on profiling MDLC of collision type as these were the most
424 amenable for our molecular profiling approaches i.e., we could clearly annotate ductal and
425 lobular tumor regions based on histological and E-cadherin staining patterns and cleanly
426 capture RNA/DNA from these individual regions. Notably, we did attempt to profile ductal and
427 lobular tumor cells separately from intermixed regions identified in MDLC-2, however, the
428 resulting data was of poor quality due to low tumor cellularity. Although our study presents a
429 unique and novel analysis of MDLC of collision type, it has some limitations, including a small
430 sample size and lack of analysis of other subtypes (such as lobular-like IBC-NST[46] and
431 intermixed/intermingled MDLC[31,44]) and tumor microenvironment of individual tumor regions
432 within MDLC. Future studies, using rapidly improving spatial sequencing technologies with
433 increased single cell capabilities will be necessary to validate and expand our observations in
434 larger and more diverse cohorts of MDLC. Generating a comprehensive MDLC cohort for future
435 studies may not be an easy task, given the challenges associated with the diagnosis of this
436 mixed entity. However, the use of E-cadherin IHC in histological assessments and evaluation by
437 a panel of pathologists can ensure the generation of a high-confidence and well-annotated
438 MDLC cohort for future studies. Moreover, the application of digital pathology and artificial
439 intelligence will make this more feasible[98]. These tools will not only improve diagnostic

accuracy[99] but will also allow scalable annotation of ductal and lobular tumor regions across heterogenous tumor samples[100].

In summary, our study provides new insights into the molecular heterogeneity of MDLC and its underlying ductal and lobular tumor regions. This is the first report on genome-wide spatially resolved and single-cell molecular profiling of MDLC. We discovered distinct biological signatures and intrinsic molecular subtypes between these regions that may have important implications for patient prognosis and clinical management. Our findings also highlight the need for comprehensive histopathological and molecular profiling of individual tumor regions within MDLC to better understand its progression and response to cytotoxic, endocrine, and other targeted therapies.

450 ## Methods

451 ### Sample Collection

452 Informed patient consent was obtained for tissue collection, and institutional review board
453 approval was obtained from the University of Pittsburgh prior to initiation of the study. Patients
454 diagnosed with "mixed invasive ductal and lobular" were identified from the UPMC Breast
455 Cancer Registry and Formalin-Fixed Paraffin-Embedded (FFPE) blocks requested from Pitt
456 Biospecimen Core. Four-um-thick FFPE sections were used for H&E, ER-alpha and E-cadherin
457 IHC staining. A panel of pathologists reviewed the H&E and E-cadherin staining to confirm
458 MDLC diagnosis in line with recent WHO guidelines[21] (10-90% of ILC and at least 10% IBC-NST)
459 and shortlisted MDLC cases amenable for multi-omic profiling i.e., those with good separation
460 of ductal and lobular tumor regions to avoid spill over and contamination of individual ductal
461 and lobular tumor regions by neighboring lobular and ductal tumor cells, respectively. Hence,
462 we selected three collision type MDLC cases that showed both clear separation of ductal and
463 lobular tumor regions along with some intermixed/intermingled regions. These included cases
464 MDLC-1, MDLC-2 & MDLC-3 (clinical features and pathology review notes are shown in
465 Supplementary Table S1A & S1B). All cases underwent NanoString digital spatial, MSK-IMPACT
466 mutation and *CDH1* promoter methylation profiling. Fresh tumor was only available for MDLC-1
467 and was utilized for single-cell RNAseq. See details in Supplementary Methods.

468 ### Multiomic Profiling

469 Digital spatial profiling (DSP) was performed using NanoString GeoMX whole transcriptome
470 atlas platform. Mutation profiling was performed using MSK-IMPACT targeted NGS panel. *CDH1*

471 promoter methylation was assessed using ddPCR system. Finally, single cell RNA sequencing
472 was performed using 10X genomics platform based on 3'end chemistry v3. Please see
473 supplementary methods for details.

474 **Multiplexed immunofluorescence**

475 Tissue sections were prepared and iteratively stained as described previously[101]. Briefly, tissue
476 sections were baked overnight at 60°C, deparaffinized with xylene, rehydrated by decreasing
477 ethanol washes, followed by proprietary antigen retrieval optimized for multiple antigens (Leica
478 Biosystems). Tissues were incubated in 0.3% Triton X-100 in PBS for 10 min followed by
479 blocking in 10% (w/v) donkey serum and 3% (w/v) bovine serum albumin (BSA) in PBS for 1 h at
480 room temperature. Primary antibodies were diluted in blocking solution and incubated for 1 h
481 at room temperature (anti-E-cadherin, Cell Signaling Technology, 96743; anti-pan-cytokeratin,
482 Millipore Sigma, C5992; anti-c-Myc Alexa Fluor 647, Abcam, ab190560; anti-p16 Alexa Fluor
483 647, Abcam, ab192054; anti-cyclin E2 Alexa Fluor 488, Abcam, ab207336; anti-cyclin A1, R&D
484 Systems, MAB7046; anti-p21, R&D Systems, AF1047; anti-phospho-H2AX Alexa Fluor 555,
485 Abcam, ab206900). In-house primary antibody fluorescent conjugates were generated using
486 the Alexa Fluor 647 labelling kit (Invitrogen, A20186) or the Alexa Fluor 555 labelling kit
487 (Invitrogen, A20187). Nuclear labelling was performed using Hoechst (2 ug/ml, Invitrogen,
488 H3570) for 10 min at room temperature. Imaging was performed in 50% glycerol (v/v) in PBS.
489 After imaging, dye inactivation was performed in an alkali solution containing H2O2 for 15 min
490 with agitation followed by a PBS wash. Samples were reimaged following dye inactivation to
491 measure residual fluorescence. Additional rounds of antibody staining and imaging were

performed as described above, starting with primary antibody incubation. Image acquisition, flat-field correction, autofluorescence removal, and registration were performed using the Cell DIVE Imager (Leica Biosystems). Single-cell segmentation was performed using Cellpose[102] and intensity measurements were extracted using scikit-image[103]. Measurements greater than 1.5x the interquartile range were identified as outliers and removed from analysis.

**Figures & Illustrations**

DSP spatial images were exported from GeoMx® Data Analysis Suite (DSPDA) and used directly in the manuscript without graphical modifications. Most bioinformatic analysis visualizations were generated using R. These visualizations were aesthetically improved in power point to produce the final figures. Illustrations were prepared using BioRender.com.

**Data Availability**

Data and code generated in this study is shared in the Supplementary Data files, Mendeley (https://data.mendeley.com/datasets/btv7g7n9ys/1) and GitHub (https://github.com/osamashiraz/MDLC_Spatial_Analysis_2023).

## Authors' Disclosures

PCL has an equity interest in Amgen (outside the submitted work). BW reports research funding by Repare Therapeutics, outside the submitted work. JSR-F reports having received personal/consultancy fees from Goldman Sachs, Bain Capital, Repare Therapeutics, Saga Diagnostics and Paige.AI, membership of the scientific advisory boards of VolitionRx, REPARE Therapeutics and Paige.AI, membership of the Board of Directors of Grupo Oncoclinicas, and ad hoc membership of the scientific advisory boards of AstraZeneca, Merck, Daiichi Sankyo, Roche Tissue Diagnostics and Personalis, outside the scope of this study. No disclosures were reported by other authors.

## Authors' Contributions

**O.S. Shah:** Conceptualization, data curation, software, formal analysis, investigation, visualization, methodology, project administration, writing–original draft, writing–review and editing. **A. Nasrazadani:** resources, funding acquisition, writing-review and editing. **J.M. Atkinson:** resources, supervision, project administration, writing–review and editing. **J. Foldi:** resources, investigation, data curation, writing–review and editing. **C.G. Kleer:** investigation, data curation, writing–review and editing. **P.F. McAuliffe:** investigation, resources, data curation, writing–review and editing. **T.J. Johnston**: investigation, resources, data curation, software, formal analysis, writing–review and editing. **W. Stallaert**: investigation, resources, data curation, software, formal analysis, writing–review and editing. **E.M. da Silva:** investigation, resources, data curation, software, formal analysis, writing–review and editing. **P. Selenica:** investigation, resources, data curation, software, formal analysis, writing–review and editing. **H. Dopeso:** investigation, resources, data curation, writing–review and editing. **F. Pareja:** investigation, resources, data curation, writing–review and editing. **D. Mandelker:** investigation, resources, data curation, writing–review and editing. **B. Weigelt:** conceptualization, investigation, methodology, resources, writing–review and editing. **J.S. Reis-Filho:** conceptualization, investigation, methodology, resources, writing–review and editing. **R. Bhargava:** conceptualization, investigation, resources, data curation, methodology, data curation, writing–review and editing. **P.C. Lucas:** conceptualization, investigation, resources, data curation, methodology, data curation, writing–review and editing. **A.V. Lee:** conceptualization, resources, methodology, supervision, funding acquisition, project

administration, writing–review and editing. **S. Oesterreich:** conceptualization, resources, methodology, supervision, funding acquisition, project administration, writing–review and editing.

## Acknowledgments

This work was primarily supported by the Dynami Foundation (Flora Migyanka) and BCRF grants to **S. Oesterreich** and in part by various other grants including the ASCO Gianni Bonadonna Breast Cancer Research Fellowship grant to **A. Nasrazadani** and Conquer Cancer ASCO Young Investigator Award to **J. Foldi**. We would also like to thank NanoString DSP Technology Access Program for providing early access to their whole transcriptome spatial technology, UPMC Hillman Cancer Center and Tissue and Research Pathology/Pitt Biospecimen Core shared resources for providing access to valuable clinical specimens and technical support (award P30CA047904), University of Pittsburgh Center for Research Computing, RRID:SCR_022735 (HTC cluster, NIH Award S10OD028483) , Pitt Genomics Research Core and UPMC Genome Center for technical support in preparing scRNAseq libraries and sequencing, and Ms. Morgan DeBerry, HTL(ASCP)CM, QIHCCM for excellent technical assistance in tissue sectioning, staining and other logistics. Research reported in this publication was partly funded by an NIH/NCI Cancer Center Support Grant (P30CA008748, MSKCC). BW, FP and JSR-F were funded in part by an NIH/NCI P50 CA247749 01 and Breast Cancer Research Foundation grants.

554 ## Figure Legends

555 **Figure 1. Digital Spatial Profiling of MDLC Ductal and Lobular Tumor Regions.** (A) Top panel
556 shows clinical timelines of the studied cases including the time of core biopsies, surgical
557 interventions, treatments, metastasis and last known vital status. The source of the tumor
558 tissue used in this study is highlighted with * in red color. The bottom panels show high (40X)
559 magnification H&E and Ecad/p120 IHC images highlighting histomorphic and E-cadherin
560 features of ductal and lobular regions across each case. (B) E-cadherin and Pan-CK
561 immunofluorescence staining of a representative case (MDLC-3). Selected regions of interests
562 (ROIs) are shown with dotted blue (for ductal) and red (for lobular). (C) Segmentation of ductal
563 and lobular cells using E-cadherin and Pan-CK staining masks. (D) Segmented areas containing
564 only ductal or lobular tumor cells defined using ductal and lobular masks illustrated in panel C.
565 (E) E-cadherin staining intensity in representative ductal and lobular regions profiled across
566 cases.

567 **Figure 2. Molecular Subtypes and Differentially Expressed Genes in Ductal and Lobular Tumor**
568 **Regions.** (A) Profiled ductal and lobular tumor regions separated by consensus clusters. All
569 regions are annotated by cases, histology, and consensus clusters. Gene expression heatmap
570 shows top variable genes and followed by PAM50 scores for each subtype across ductal and
571 lobular regions. (B) Differentially expressed genes (DEGs) between ER+ ductal and lobular
572 regions. The top panel shows DEG heatmap, while bottom panel shows volcano plot along with
573 number of significantly upregulated (N=168) and downregulated (N=198) DEGs in ductal vs
574 lobular regions.

575 **Figure 3. Distinct Hallmark and Biological Signatures in Ductal and Lobular Tumor Regions.** (A)
576 Differentially enriched cancer hallmark signatures. The heatmap shows GSVA scores of each
577 differentially enriched pathway in ductal vs lobular tumor regions. Pathways with bold red and
578 blue names are the ones that also were significant in the scRNAseq dataset (Supplementary Fig.
579 S8A). Enrichment score (ES) for a pathway shows mean differences of GSVA score for that
580 pathway in lobular – ductal regions and the -log10 of FDR-adjusted P-value (P-val) shows
581 statistical significance of enrichment based on T test. (P-val score definitions: 4 = P ≤ 0.0001, 3 =
582 P ≤ 0.001, 2 = P ≤ 0.01 and 1 = P ≤ 0.05). (B) The heatmap shows GSVA scores of differentially
583 enriched signatures between TCGA ER+ IBC-NST vs. ILC that overlap with MDLC ductal vs lobular
584 tumor region hallmark signatures in panel A. (C) Recurrent biological themes in ductal and
585 lobular tumor regions. The left panel shows the Jaccard similarity between all signatures.
586 Signatures are grouped based on their Jaccard similarity into signature clusters. Each cluster is
587 associated with a broad biological theme (shown in middle). The right panel shows the mean
588 GSVA score of each signature cluster in ductal and lobular regions. (D) E-cadherin (ECad) and
589 pan-cytokeratin (pan-CK26) staining in representative image of adjacent ductal and lobular
590 tumor regions. (E) Representative immunofluorescence images (right panel) and single-cell
591 quantification (left panel) of cell cycle and senescence biomarkers from all ER+ ductal and
592 lobular regions. Statistical significance is determined using a student's t-test (****: P ≤ 0.0001).
593 ECM: Extracellular matrix, DSB: Double stranded break, HR: Homologous recombination.

594 **Figure 4. Overview of Genomic Alterations in Ductal and Lobular Tumor Regions.** (A) Somatic
595 mutations identified using MSK-IMPACT panel in ductal and lobular components across

samples. Gene names are followed by amino acid change due to mutation. Genes in black font had somatic mutations in breast cancer driver genes while those in gray color had passenger/non-driver mutations. (B) Somatic copy number changes in ductal and lobular components across samples. For each case, genome-wide ductal and lobular copy number profiles are shown. Black line shows total copy number, red line shows minor allele copy number and off-white regions show aneuploidy (change in minor allele copy number including LOH). (C) Mutational signatures in MDLC-2 and MDCL-3 ductal and lobular tumor regions. Pie charts show percentage similarity of mutational patterns of each tumor component with established mutational patterns (associated with different means/definition). (D) Predicted disease evolution. Tumors with overlapping mutations were linked to common root node indicating common progenitor or precursor neoplasm (N). Those without common root node likely indicate evolution from independent precursors. Key mutations and events (*CDH1* promoter methylation and amplifications) are shown on the branches.

**Figure 5: Single Cell Heterogeneity of Ductal and Lobular Tumor Populations.** (A) Tumor populations in MDLC-1 scRNAseq dataset (left) and assessment of CDH1 expression in MDLC-1 scRNAseq dataset (middle and right plot). Statistical significance was evaluated using the T test. (B) Deconvolution of scRNAseq using DSP derived ductal and lobular signatures. GSVA scores for ductal and lobular signatures are shown on the right panel. (C) Sub-clustering and identification of ductal and lobular sub-populations (left) with unique marker genes (right). (D) Scoring spatial regions using GSVA of sub-cluster marker genes. (E) Mapping of single cell populations to spatial regions based on GSVA scores in panel D.

## Supplementary Figure Legends

**Supplementary Figure S1: Digital Spatial Profiling RNAseq Dataset Quality Control.** (A) Scatter plot showing sequencing saturation (y-axis) and area of interest (AOI) surface area (mm2) across cases. Dashed red lines show the quality control (QC) cutoffs (sequencing saturation >50% and area > 6000mm$^2$) for selecting high quality samples. (B) Overview of signal (Q3-normalized counts) to noise (negative probe counts). Dashed red line shows cutoff i.e., signal > noise. (C) Evaluation of Q3 normalized counts (for 1000 randomly sampled genes) across profiled regions to identify samples with low quality data showing count artifacts. (D) tSNE plot showing clustering of profiled samples that passed QC cutoffs. (E) *CDH1, ESR1, ERBB2* and *PGR* gene expression in ductal vs lobular regions across the three profiled cases. Statistical significance was evaluated using the T test. (F) Expression of EMT marker genes in ductal and lobular tumor regions across each case. EMT marker genes were adapted from McCart Reed et al[34].

**Supplementary Figure S2: Patient Wise and Pan-Patient MDLC Ductal vs Lobular Differential Analysis.** Volcano plots (top) showing per patient or patient-wise differentially expressed genes (DEGs) between ductal vs lobular tumor regions and overlap of these patient-wise DEGs with pan-patient (all patients combined) DEGs for (A) MDLC-1, (B) MDLC-2 and (C) MDLC-3. A RF > 1 and p < 0.01 shows significantly strong overlap. (D) Overlap of MDLC pan-patient ductal vs. lobular DEGs with TCGA ER+ IBC-NST vs ILC DEGs. Statistical significance of overlap between genesets was computed using overlap_stats tool (http://nemates.org/MA/progs/overlap_stats.html). RF: Representation Factor. For details on

638 RF calculation see overlap_stats webpage. Briefly, RF is the number of overlapping genes
639 divided by the expected number of overlapping genes drawn from two independent groups. A
640 RF > 1 indicates more overlap than expected for independent genesets, a RF < 1 indicates less
641 overlap than expected, and a RF = 1 indicates that the two genesets by the number of genes
642 expected for independent groups of genes.

643 **Supplementary Figure S3: Transcription Factor Enrichment Analysis using Pan-Patient Ductal**
644 **vs Lobular DEGs.** Ductal vs Lobular DEGs were separately input into eXpression2Kinase (X2K)
645 web tool (https://maayanlab.cloud/X2K/) to identify enriched transcription factors and kinases
646 in ductal (left) and lobular (right) tumor regions. The top layer with blue nodes shows kinases,
647 middle layer shows intermediate proteins and bottom layer with red nodes shows transcription
648 factors. An image inset is shown highlighting MYC and ER signaling related transcription factors
649 enriched in ductal and lobular tumor regions, respectively.

650 **Supplementary Figure S4: Key Genes Associated with Notable Differentially Enriched**
651 **Oncogenic and Biological Signatures.** (A) Venn diagram showing overlap between D1: Double
652 stranded break/homologous recombination (DBS/HR), Hallmark G2m Checkpoint and Hallmark
653 Myc Targets V1. (B). Venn diagram showing overlap between Hallmark Myc Targets V1, L1: Cell
654 Cycle and L2: TP53 & Senescence. Details of all genes in each signature shown in (A) and (B) are
655 listed in Supplementary Tables S6 and S7. The genes used for comparing biological theme
656 signature clusters (D1: DBS/HR, L1: Cell Cycle and L2: TP53 & Senescence) are defined as union
657 of all individual signatures present in each of these signature clusters. (C) Expression of select
658 genes from Hallmark Myc Targets V1, L1: Cell Cycle, L2: TP53/Senescence, L5: Collagen & ECM,

659 L7: Collagen metabolism, L9: MAPK/ERK Targets, and D5: mTOR in ductal vs. lobular tumor
660 regions. Statistical significance was evaluated using the T test.

661 **Supplementary Figure S5: MSK-IMPACT Extended Results.** (A) Tumor purity, sequencing
662 coverage and ploidy of ductal and lobular tumor regions across profiled cases. (B) Somatic
663 mutations and their cancer cell fraction (CCF). High CCF indicate clonal mutations while low CCF
664 indicates sub-clonal mutations. (C) Copy number of key breast cancer genes in ductal vs lobular
665 regions across each case.

666 **Supplementary Figure S6: Effect of Q23 mutation on CDH1 RNA and E-cadherin protein**
667 **expression in ER+ Breast Tumors.** Bar plots showing CDH1 RNA (top) and E-cadherin protein
668 (bottom) expression in ER+ patient tumor samples (N=434) with CDH1 Q23* mutations (N=5),
669 all other CDH1 truncating mutations (N=71) and CDH1 WT (N=358) in ER+ breast tumors in
670 TCGA cohort. To avoid confounding effects of CDH1 copy number, we excluded all tumor
671 samples with CDH1 gains, amplification, and deep deletions. Statistical significance is
672 determined using student's t-test (****: $P \leq 0.0001$, **: $P \leq 0.01$).

673 **Supplementary Figure S7: MDLC-1 Ductal and Lobular Tumor scRNAseq Heterogeneity.** (A)
674 MDLC-1 single-cell RNAseq (scRNAseq) dataset quality control metrics from cell ranger
675 software. (B) tSNE plot showing identified cell types in the scRNAseq dataset including T-cells,
676 Endothelial cells (Endo), Macrophages (Macro), Fibroblasts (Fibro), Smooth muscle cells,
677 luminal tumor epithelial cells (Tumor cells), luminal epithelial cells (Luminal cells) and basal
678 epithelial cells (Basal cells). (C) CopyKat algorithm predictions for copy number status of
679 scRNAseq dataset to confirm aneuploidy status of tumor cells and diploid status of non-tumor

cells. (D) MDLC-1 scRNAseq ductal vs lobular DEG analysis. (E) Heatmap of CopyKat inferred copy number values for ductal and lobular tumor cell populations. (F) Overlap of MDLC-1 ductal vs lobular DEGs between scRNAseq and digital spatial profiling (DSP) datasets. A RF > 1 and p < 0.01 shows significantly strong overlap. Statistical significance of DEG overlap between DEGs from two technologies was computed using overlap_stats tool as described previously in Supplementary Fig. S2. (G) Top five marker genes of each ductal and lobular sub-cluster identified in Fig. 5C.

**Supplementary Figure S8: Distinct Biological Signatures in MDLC-1 Ductal and Lobular Tumor scRNAseq.** (A) GSVA based hallmark signature enrichment analysis in scRNAseq dataset. Enrichment score (ES) for a pathway shows mean differences of GSVA score for that pathway in lobular – ductal regions and the -log10 of FDR-adjusted P-value (P-val) shows statistical significance of enrichment based on T test. (P-val score definitions: 4 = P ≤ 0.0001, 3 = P ≤ 0.001, 2 = P ≤ 0.01 and 1 = P ≤ 0.05). (B) Barplots showing mean GSVA scores of hallmark signatures in ductal and lobular subclusters. (C) Recurring biology themes in ductal vs lobular cells in scRNAseq dataset. (D) Mean GSVA score for select differentially enriched biology themes across ductal and lobular sub-clusters.

## References


1. Bray, F. *et al.* Global cancer statistics 2018: GLOBOCAN estimates of incidence and mortality worldwide for 36 cancers in 185 countries. **68**, 394–424 (2018).
2. Siegel, R. L., Miller, K. D., Wagle, N. S. & Jemal, A. Cancer statistics, 2023. *CA Cancer J Clin* **73**, 17–48 (2023).
3. Sledge, G. W., Chagpar, A. & Perou, C. Collective wisdom: lobular carcinoma of the breast. *Am Soc Clin Oncol Educ B* **35**, 18–21 (2016).
4. Reed, M. E. M. C., Kutasovic, J. R., Lakhani, S. R. & Simpson, P. T. Invasive lobular carcinoma of the breast: morphology, biomarkers and ’omics. **17**, 12 (2015).
5. Ciriello, G. *et al.* Comprehensive molecular portraits of invasive lobular breast cancer. *Cell* **163**, 506–519 (2015).
6. Reed, M. E. M. C., Kutasovic, J. R., Lakhani, S. R. & Simpson, P. T. Invasive lobular carcinoma of the breast: morphology, biomarkers and ’omics. **17**, 12 (2015).
7. Dabbs, D. J., Bhargava, R. & Chivukula, M. Lobular versus ductal breast neoplasms: the diagnostic utility of p120 catenin. *Am J Surg Pathol* **31**, 427–37 (2007).
8. Arpino, G. *et al.* Infiltrating lobular carcinoma of the breast: tumor characteristics and clinical outcome. **6**, (2004).
9. Oesterreich, S. *et al.* Clinicopathological Features and Outcomes Comparing Patients With Invasive Ductal and Lobular Breast Cancer. *J Natl Cancer Inst* **114**, 1511–1522 (2022).
10. Z, C. *et al.* Invasive lobular carcinoma of the breast: A special histological type compared with invasive ductal carcinoma. **12**, e0182397 (2017).
11. Yeatman, T. J. *et al.* Tumor biology of infiltrating lobular carcinoma. Implications for management. *Ann Surg* **222**, 549–559 (1995).
12. Helvie, M. A., Paramagul, C., Anderson, K. L. & Adler, D. D. Invasive lobular carcinoma. Imaging features and clinical detection. *Invest Radiol* **28**, 202–207 (1993).
13. Arpino, G. *et al.* Infiltrating lobular carcinoma of the breast: tumor characteristics and clinical outcome. **6**, (2004).
14. Oesterreich, S. *et al.* Clinicopathological Features and Outcomes Comparing Patients With Invasive Ductal and Lobular Breast Cancer. *J Natl Cancer Inst* **114**, 1511–1522 (2022).
15. Mathew, A. *et al.* Distinct Pattern of Metastases in Patients with Invasive Lobular Carcinoma of the Breast. *Geburtshilfe Frauenheilkd* (2017) doi:10.1055/s-0043-109374.
16. Lamovec, J. & Bračkko, M. Metastatic pattern of infiltrating lobular carcinoma of the breast: an autopsy study. **48**, 28–33 (1991).
17. Djerroudi, L., Cabel, L., Bidard, F. C. & Vincent-Salomon, A. Invasive Lobular Carcinoma of the Breast: Toward Tailoring Therapy? **114**, 1434–1436 (2022).
18. K, V. B. *et al.* Current and future diagnostic and treatment strategies for patients with invasive lobular breast cancer. *Annals of Oncology* **33**, 769–785 (2022).

19. Luveta, J., Parks, R. M., Heery, D. M., Cheung, K.-L. & Johnston, S. J. Invasive Lobular Breast Cancer as a Distinct Disease: Implications for Therapeutic Strategy. *Oncol Ther* **8**, 1–11 (2020).

20. K, V. B. *et al.* Current and future diagnostic and treatment strategies for patients with invasive lobular breast cancer. *Annals of Oncology* **33**, 769–785 (2022).

21. Hoon Tan, P. *et al.* The 2019 WHO classification of tumours of the breast. *Histopathology* (2020) doi:10.1111/his.14091.

22. Sinn, H. P. & Kreipe, H. *A Brief Overview of the WHO Classification of Breast Tumors, 4th Edition, Focusing on Issues and Updates from the 3rd Edition*. *Breast Care* vol. 8 149 (Karger Publishers, 2013).

23. Metzger-Filho, O. *et al*. *The Diagnosis of Mixed Invasive Ductal and Lobular Carcinoma (IDC-L) in Clinical Practice Is Often Associated with Uncertainty Related to Its Prognosis and Response to Systemic Therapies. With the Increasing Recognition of Invasive Lobular Carc*. vol. 24 (Oxford University Press (OUP), 2019).

24. Zengel, B. *et al.* Comparison of the clinicopathological features of invasive ductal, invasive lobular, and mixed (invasive ductal + invasive lobular) carcinoma of the breast. *Breast Cancer* (2015) doi:10.1007/s12282-013-0489-8.

25. Xiao, Y. *et al.* Mixed invasive ductal and lobular carcinoma has distinct clinical features and predicts worse prognosis when stratified by estrogen receptor status. *Sci Rep* (2017) doi:10.1038/s41598-017-10789-x.

26. Duraker, N., Hot, S., Akan, A. & Ozay Nayir, P. A Comparison of the Clinicopathological Features, Metastasis Sites and Survival Outcomes of Invasive Lobular, Invasive Ductal and Mixed Invasive Ductal and Lobular Breast Carcinoma. *Eur J Breast Health* **16**, 22–31 (2020).

27. Nasrazadani, A. *et al.* Mixed invasive ductal lobular carcinoma is clinically and pathologically more similar to invasive lobular than ductal carcinoma. *British Journal of Cancer 2023* 1–10 (2023) doi:10.1038/s41416-022-02131-8.

28. Ciriello, G. *et al.* Comprehensive molecular portraits of invasive lobular breast cancer. *Cell* **163**, 506–519 (2015).

29. Nasrazadani, A. *et al.* Mixed invasive ductal lobular carcinoma is clinically and pathologically more similar to invasive lobular than ductal carcinoma. *British Journal of Cancer 2023* 1–10 (2023) doi:10.1038/s41416-022-02131-8.

30. Lohani, K. R. *et al.* Lobular-Like Features and Outcomes of Mixed Invasive Ductolobular Breast Cancer (MIDLC): Insights from 54,403 Stage I-III MIDLC Patients. *Ann Surg Oncol* **31**, 936–946 (2024).

31. Pérez-Mies, B. *et al*. The Clonal Relationship Between the Ductal and Lobular Components of Mixed Ductal-Lobular Carcinomas Suggested a Ductal Origin in Most Tumors. *American Journal of Surgical Pathology* **46**, 1545–1553 (2022).

32. Li, C. I., Anderson, B. O., Daling, J. R. & Moe, R. E. Trends in Incidence Rates of Invasive Lobular and Ductal Breast Carcinoma. *J Am Med Assoc* (2003) doi:10.1001/jama.289.11.1421.

33. Suryadevara, A., Paruchuri, L. P., Banisaeed, N., Dunnington, G. & Rao, K. A. The clinical behavior of mixed ductal/lobular carcinoma of the breast: A clinicopathologic analysis. *World J Surg Oncol* (2010) doi:10.1186/1477-7819-8-51.

34. Rakha, E. A. *et al.* The biological and clinical characteristics of breast carcinoma with mixed ductal and lobular morphology. *Breast Cancer Res Treat* (2009) doi:10.1007/s10549-008-0007-4.

35. Acs, G., Lawton, T. J., Rebbeck, T. R., LiVolsi, V. A. & Zhang, P. J. Differential Expression of E-Cadherin in Lobular and Ductal Neoplasms of the Breast and Its Biologic and Diagnostic Implications. *Am J Clin Pathol* (2001) doi:10.1309/FDHX-L92R-BATQ-2GE0.

36. McCart Reed, A. E. *et al.* Mixed ductal-lobular carcinomas: evidence for progression from ductal to lobular morphology. *Journal of Pathology* (2018) doi:10.1002/path.5040.

37. Christgen, M. *et al.* Inter-observer agreement for the histological diagnosis of invasive lobular breast carcinoma. *J Pathol Clin Res* **8**, 191–205 (2022).

38. Metzger□Filho, O. *et al.* Mixed Invasive Ductal and Lobular Carcinoma of the Breast: Prognosis and the Importance of Histologic Grade. *Oncologist* **24**, (2019).

39. Zhao, H. The prognosis of invasive ductal carcinoma, lobular carcinoma and mixed ductal and lobular carcinoma according to molecular subtypes of the breast. *Breast Cancer* **28**, 187–195 (2021).

40. Arps, D. P., Healy, P., Zhao, L., Kleer, C. G. & Pang, J. C. Invasive ductal carcinoma with lobular features: a comparison study to invasive ductal and invasive lobular carcinomas of the breast. *Breast Cancer Res Treat* **138**, 719 (2013).

41. Zels, G. *et al.* Metastases of primary mixed no-special type and lobular breast cancer display an exclusive lobular histology. *Breast* **75**, 103732 (2024).

42. M, C. *et al.* Lobular breast cancer: Histomorphology and different concepts of a special spectrum of tumors. **13**, 3695 (2021).

43. Christgen, M., Kandt, L. D., Antonopoulos, W. & al., et. Inter-observer agreement for the histological diagnosis of invasive lobular breast carcinoma. *J Pathol Clin Res* **8**, 191–205 (2022).

44. Tang, X. *et al.* Mixed ductal–lobular carcinoma: an analysis of CDH1 DNA copy number variation and mutation. *Breast Cancer* **28**, 1318–1327 (2021).

45. McCart Reed, A. E. *et al.* Mixed ductal-lobular carcinomas: evidence for progression from ductal to lobular morphology. *Journal of Pathology* (2018) doi:10.1002/path.5040.

46. Yu, J. *et al.* Clinicopathologic and genomic features of lobular like invasive mammary carcinoma: is it a distinct entity? *npj Breast Cancer 2023 9:1* **9**, 1–13 (2023).

47. Ciriello, G. *et al.* Comprehensive Molecular Portraits of Invasive Lobular Breast Cancer. *Cell* **163**, 506–519 (2015).

48. Suryadevara, A., Paruchuri, L. P., Banisaeed, N., Dunnington, G. & Rao, K. A. The clinical behavior of mixed ductal/lobular carcinoma of the breast: A clinicopathologic analysis. *World J Surg Oncol* (2010) doi:10.1186/1477-7819-8-51.

49. Pérez-Mies, B. *et al.* The Clonal Relationship Between the Ductal and Lobular Components of Mixed Ductal-Lobular Carcinomas Suggested a Ductal Origin in Most Tumors. *American Journal of Surgical Pathology* **46**, 1545–1553 (2022).

50. Liberzon, A. *et al.* The Molecular Signatures Database Hallmark Gene Set Collection. *Cell Syst* **1**, 417–425 (2015).

51. Carbon, S. *et al.* The Gene Ontology resource: enriching a GOld mine. *Nucleic Acids Res* **49**, D325–D334 (2021).

52. Gillespie, M. *et al.* The reactome pathway knowledgebase 2022. *Nucleic Acids Res* **50**, D687–D692 (2022).

53. Kanehisa, M., Furumichi, M., Sato, Y., Kawashima, M. & Ishiguro-Watanabe, M. KEGG for taxonomy-based analysis of pathways and genomes. *Nucleic Acids Res* **51**, D587–D592 (2023).

54. Cleton-Jansen, A. M. E-cadherin and loss of heterozygosity at chromosome 16 in breast carcinogenesis: different genetic pathways in ductal and lobular breast cancer? *Breast Cancer Res* **4**, 5–8 (2002).

55. André, F. *et al.* Alpelisib for PIK3CA -Mutated, Hormone Receptor–Positive Advanced Breast Cancer . *New England Journal of Medicine* **380**, 1929–1940 (2019).

56. Theodorou, V., Stark, R., Menon, S. & Carroll, J. S. GATA3 acts upstream of FOXA1 in mediating ESR1 binding by shaping enhancer accessibility. *Genome Res* **23**, 12 (2013).

57. Malik, N. *et al.* The transcription factor CBFB suppresses breast cancer through orchestrating translation and transcription. *Nature Communications 2019 10:1* **10**, 1–15 (2019).

58. Comprehensive molecular portraits of human breast tumours. *Nature* **490**, (2012).

59. Gala, K. *et al.* KMT2C mediates the estrogen dependence of breast cancer through regulation of ERα enhancer function. *Oncogene 2018 37:34* **37**, 4692–4710 (2018).

60. Glaser, A. P. *et al.* APOBEC-mediated mutagenesis in urothelial carcinoma is associated with improved survival, mutations in DNA damage response genes, and immune response. *Oncotarget* **9**, 4537–4548 (2017).

61. Shen, R. & Seshan, V. E. FACETS: allele-specific copy number and clonal heterogeneity analysis tool for high-throughput DNA sequencing. *Nucleic Acids Res* **44**, (2016).

62. Glaser, A. P. *et al.* APOBEC-mediated mutagenesis in urothelial carcinoma is associated with improved survival, mutations in DNA damage response genes, and immune response. *Oncotarget* **9**, 4537–4548 (2017).

63. Klonowski, J., Liang, Q., Coban-Akdemir, Z., Lo, C. & Kostka, D. aenmd: annotating escape from nonsense-mediated decay for transcripts with protein-truncating variants. *Bioinformatics* **39**, (2023).

64. Khajavi, M., Inoue, K. & Lupski, J. R. Nonsense-mediated mRNA decay modulates clinical outcome of genetic disease. *European Journal of Human Genetics 2006 14:10* **14**, 1074–1081 (2006).

65. Litchfield, K. *et al.* Escape from nonsense-mediated decay associates with anti-tumor immunogenicity. *Nature Communications 2020 11:1* **11**, 1–11 (2020).

66. Moffitt, J. R., Lundberg, E. & Heyn, H. The emerging landscape of spatial profiling technologies. *Nature Reviews Genetics 2022 23:12* **23**, 741–759 (2022).

67. van Amerongen, R. Behind the Scenes of the Human Breast Cell Atlas Project. *J Mammary Gland Biol Neoplasia* **26**, 67 (2021).

68. Nguyen, Q. H. *et al.* Profiling human breast epithelial cells using single cell RNA sequencing identifies cell diversity. *Nat Commun* (2018) doi:10.1038/s41467-018-04334-1.

69. Gray, G. K. *et al.* A human breast atlas integrating single-cell proteomics and transcriptomics. *Dev Cell* **57**, 1400-1420.e7 (2022).

70. Wu, S. Z. *et al.* A single-cell and spatially resolved atlas of human breast cancers. *Nature Genetics 2021 53:9* **53**, 1334–1347 (2021).

71. Sun, H. *et al.* The relevance between hypoxia-dependent spatial transcriptomics and the prognosis and efficacy of immunotherapy in claudin-low breast cancer. *Front Immunol* **13**, 7828 (2023).

72. Bassiouni, R. *et al.* Spatial Transcriptomic Analysis of a Diverse Patient Cohort Reveals a Conserved Architecture in Triple-Negative Breast Cancer. *Cancer Res* **83**, 34–48 (2023).

73. Johnson, B. E. *et al.* An omic and multidimensional spatial atlas from serial biopsies of an evolving metastatic breast cancer. *Cell Rep Med* **3**, 100525 (2022).

74. Kulasinghe, A. *et al.* Spatial Profiling Identifies Prognostic Features of Response to Adjuvant Therapy in Triple Negative Breast Cancer (TNBC). *Front Oncol* **11**, 1 (2021).

75. Andersson, A. *et al.* Spatial deconvolution of HER2-positive breast cancer delineates tumor-associated cell type interactions. *Nature Communications 2021 12:1* **12**, 1–14 (2021).

76. Badve, S. *et al.* Basal-like and triple-negative breast cancers: a critical review with an emphasis on the implications for pathologists and oncologists. *Modern Pathology* **24**, 157–167 (2011).

77. Perou, C. M. Molecular Stratification of Triple□Negative Breast Cancers. *Oncologist* **16**, 61–70 (2011).

78. Michaut, M. *et al.* Integration of genomic, transcriptomic and proteomic data identifies two biologically distinct subtypes of invasive lobular breast cancer. *Sci Rep* (2016) doi:10.1038/srep18517.

79. Djerroudi, L., Cabel, L., Bidard, F. C. & Vincent-Salomon, A. Invasive Lobular Carcinoma of the Breast: Toward Tailoring Therapy? **114**, 1434–1436 (2022).

80. Gulhan, D. C., Lee, J. J. K., Melloni, G. E. M., Cortés-Ciriano, I. & Park, P. J. Detecting the mutational signature of homologous recombination deficiency in clinical samples. *Nat Genet* **51**, 912–919 (2019).

81. Alexandrov, L. B. *et al.* Signatures of mutational processes in human cancer. *Nature* **500**, 415–421 (2013).

82. Alexandrov, L. B. *et al.* The repertoire of mutational signatures in human cancer. *Nature* **578**, 94–101 (2020).

83. Vahdatinia, M. *et al.* KIT genetic alterations in breast cancer. *J Clin Pathol* (2022) doi:10.1136/JCP-2022-208611.

84. Geyer, F. C. *et al.* Genetic analysis of a morphologically heterogeneous ovarian endometrioid carcinoma. *Histopathology* **71**, 480 (2017).

85. Azim, H. A., Nguyen, B., Brohée, S., Zoppoli, G. & Sotiriou, C. Genomic aberrations in young and elderly breast cancer patients. *BMC Med* **13**, 1–7 (2015).

86. Afzaljavan, F., Sadr, A. S., Savas, S. & Pasdar, A. GATA3 somatic mutations are associated with clinicopathological features and expression profile in TCGA breast cancer patients. *Scientific Reports 2021 11:1* **11**, 1–13 (2021).

87. BeLow, M. & Osipo, C. Notch Signaling in Breast Cancer: A Role in Drug Resistance. *Cells 2020, Vol. 9, Page 2204* **9**, 2204 (2020).

88. Hopkins, J. L., Lan, L. & Zou, L. DNA repair defects in cancer and therapeutic opportunities. *Genes Dev* **36**, 278 (2022).

89. Voutsadakis, I. A. & Stravodimou, A. Homologous Recombination Defects and Mutations in DNA Damage Response (DDR) Genes Besides BRCA1 and BRCA2 as Breast Cancer Biomarkers for PARP Inhibitors and Other DDR Targeting Therapies. *Anticancer Res* **43**, 967–981 (2023).

90. McCart Reed, A. E. *et al.* An epithelial to mesenchymal transition programme does not usually drive the phenotype of invasive lobular carcinomas. *Journal of Pathology* **238**, 489–494 (2016).

91. Herschkowitz, J. I. *et al.* Identification of conserved gene expression features between murine mammary carcinoma models and human breast tumors. *Genome Biol* **8**, 1–17 (2007).

92. Pan, C. *et al.* Research progress of Claudin-low breast cancer. *Front Oncol* **13**, 1226118 (2023).

93. Dias, K. *et al.* Claudin-Low Breast Cancer; Clinical & Pathological Characteristics. *PLoS One* **12**, (2017).

94. McCart Reed, A. E. *et al.* Mixed ductal-lobular carcinomas: evidence for progression from ductal to lobular morphology. *Journal of Pathology* (2018) doi:10.1002/path.5040.

95. Kutasovic, J. R., McCart Reed, A. E., Sokolova, A., Lakhani, S. R. & Simpson, P. T. Morphologic and genomic heterogeneity in the evolution and progression of breast cancer. *Cancers* vol. 12 Preprint at https://doi.org/10.3390/cancers12040848 (2020).

96. Ciriello, G. *et al.* Comprehensive Molecular Portraits of Invasive Lobular Breast Cancer. *Cell* (2015) doi:10.1016/j.cell.2015.09.033.

97. Bajrami, I. *et al.* E-Cadherin/ROS1 Inhibitor Synthetic Lethality in Breast Cancer. *Cancer Discov* **8**, 498–515 (2018).

98. Jiang, Y., Yang, M., Wang, S., Li, X. & Sun, Y. Emerging role of deep learning-based artificial intelligence in tumor pathology. *Cancer Commun* **40**, 154–166 (2020).

99. Couture, H. D. *et al.* Image analysis with deep learning to predict breast cancer grade, ER status, histologic subtype, and intrinsic subtype. *npj Breast Cancer 2018 4:1* **4**, 1–8 (2018).

100. Chan, R. C. K. *et al.* Artificial intelligence in breast cancer histopathology. *Histopathology* **82**, 198–210 (2023).

101. Gerdes, M. J. *et al.* Highly multiplexed single-cell analysis of formalin-fixed, paraffin-embedded cancer tissue. *Proc Natl Acad Sci U S A* **110**, 11982–11987 (2013).

102. Pachitariu, M. & Stringer, C. Cellpose 2.0: how to train your own model. *Nat Methods* **19**, 1634–1641 (2022).

103. Van Der Walt, S. *et al*. scikit-image: image processing in Python. *PeerJ* **2**, (2014).

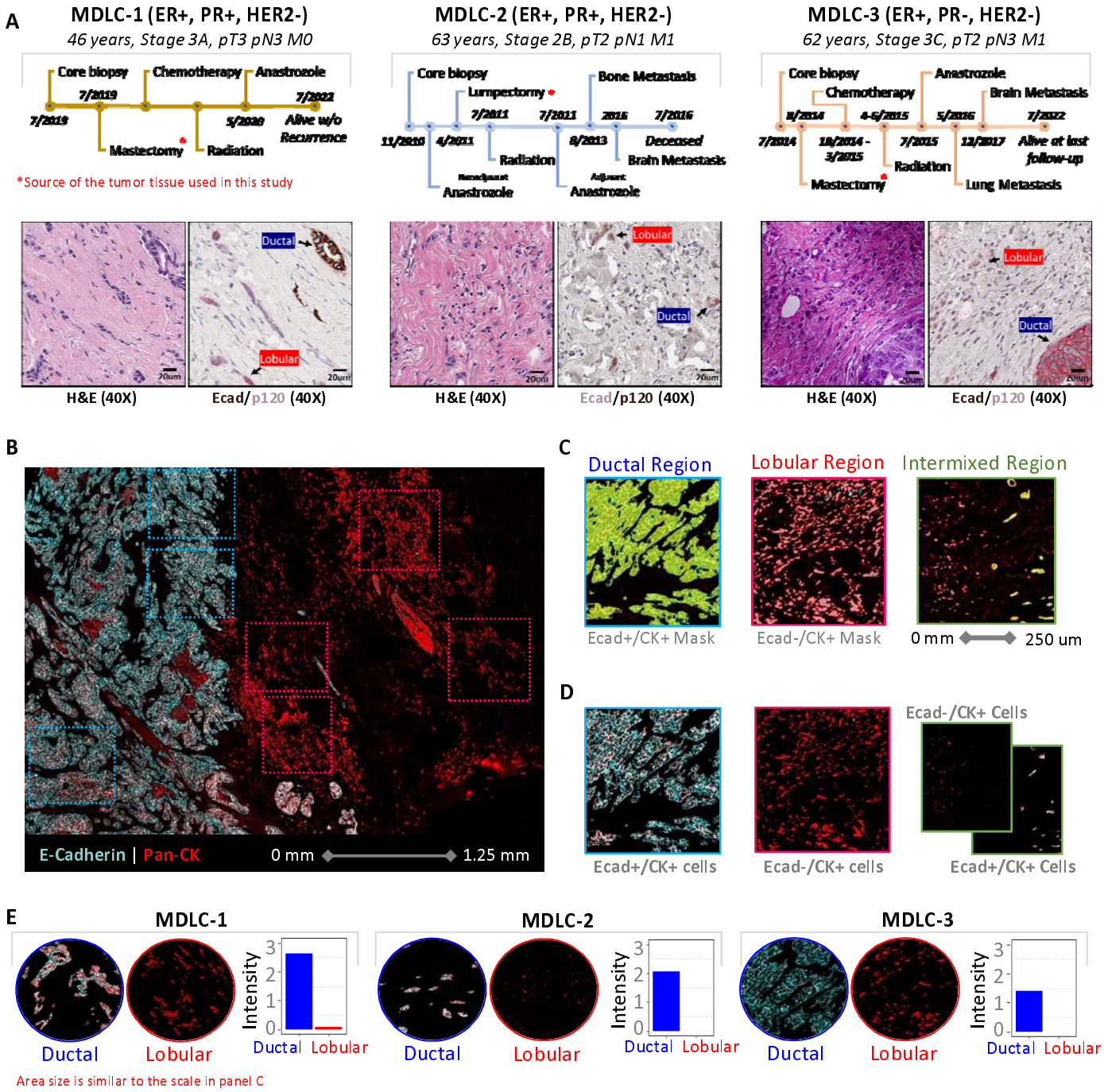


**Figure 1. Digital Spatial Profiling of mDLC Ductal and Lobular Tumor Regions.**

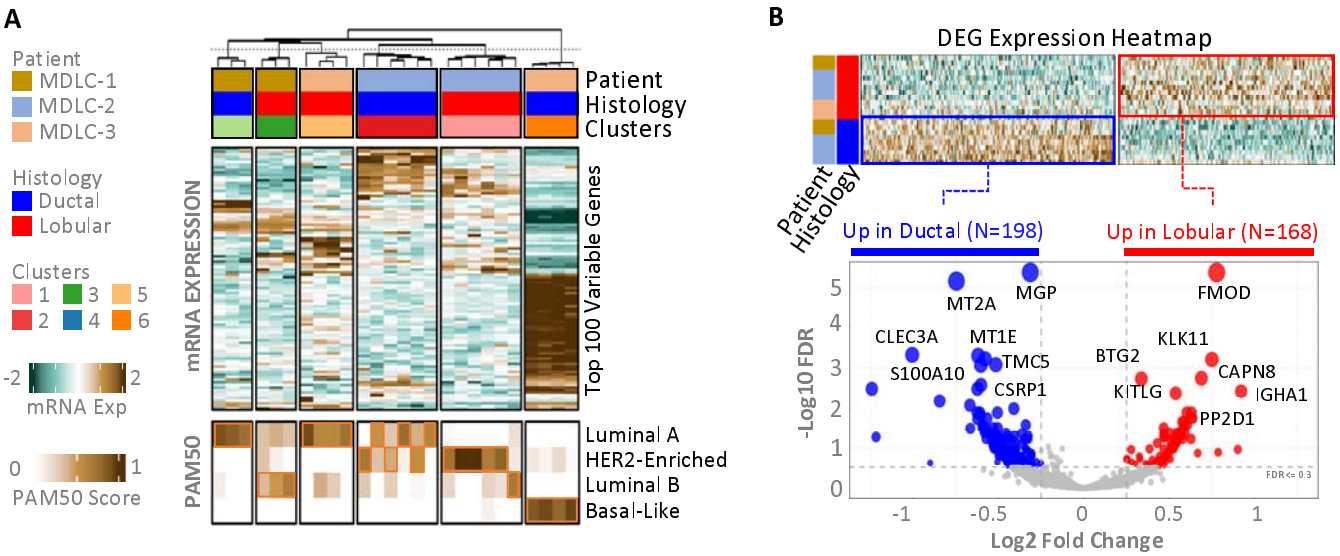


**Figure 2. Molecular Subtypes and Differentially Expressed Genes in Ductal and Lobular Tumor Regions.**

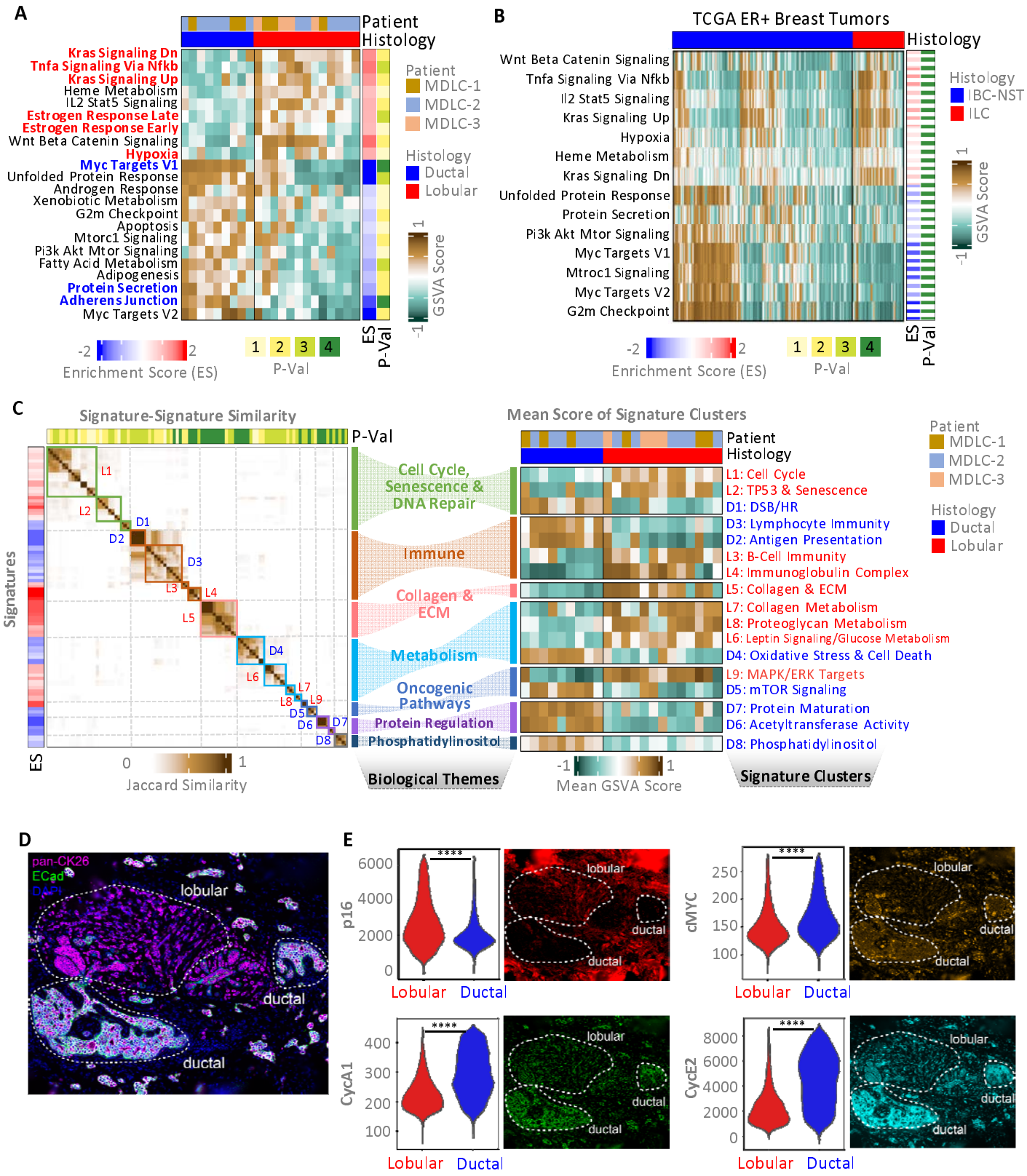


**Figure 3. Distinct Biological Signatures in Ductal and Lobular Tumor Regions**

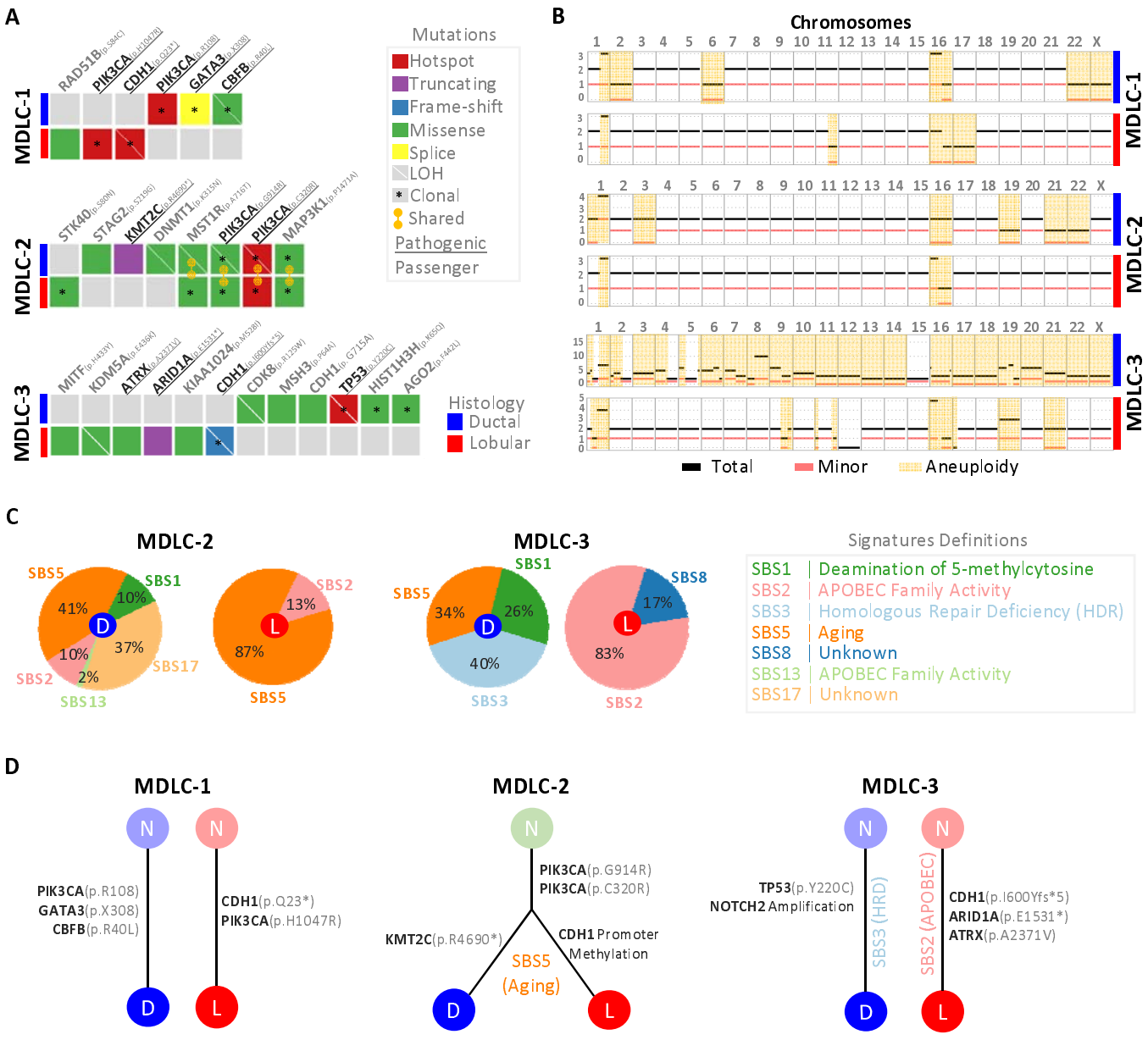


**Figure 4. Overview of Genomic Alterations in Ductal and Lobular Tumor Regions.**

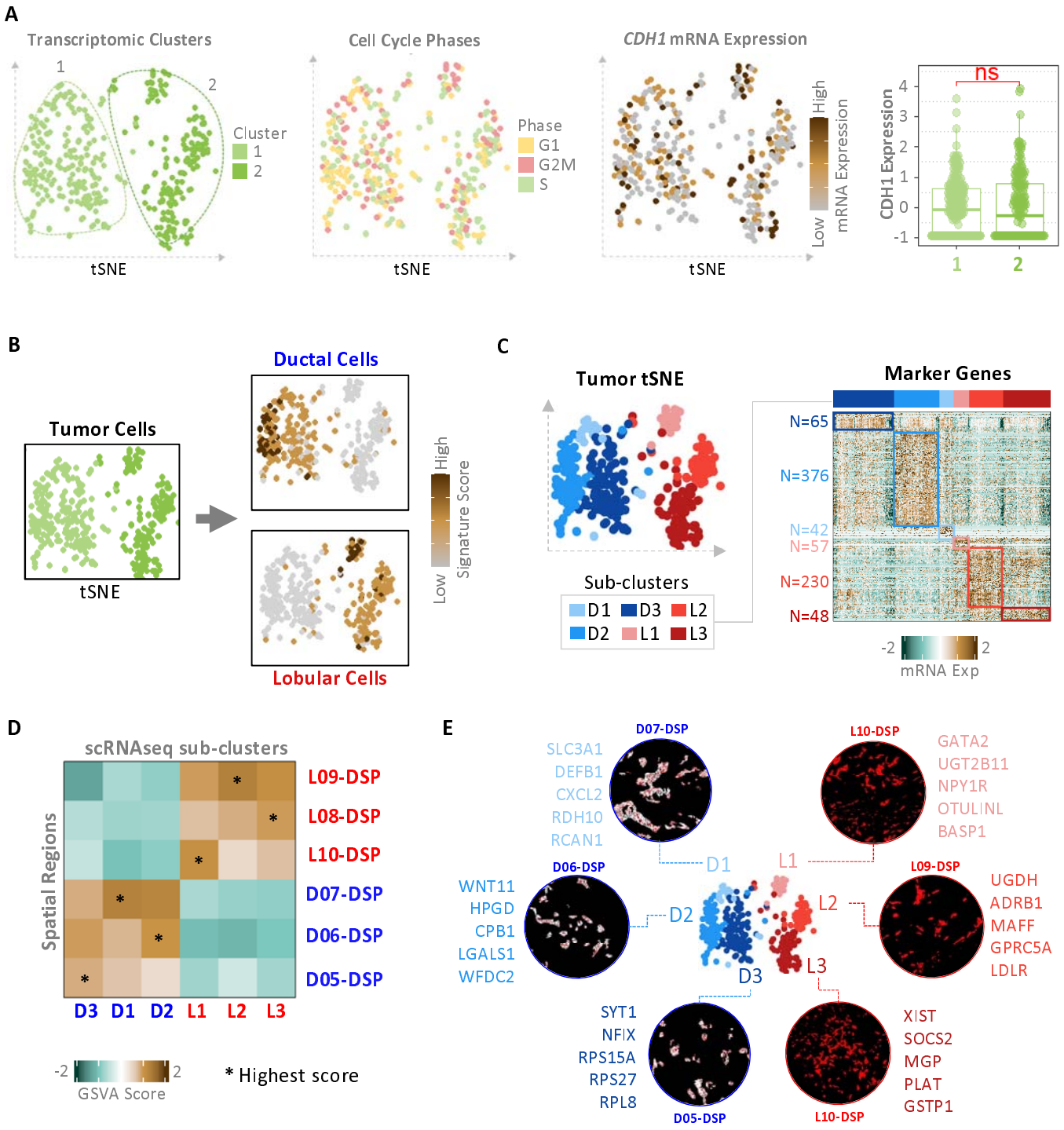


**Figure 5: Single Cell Heterogeneity of Ductal and Lobular Tumor Populations.**

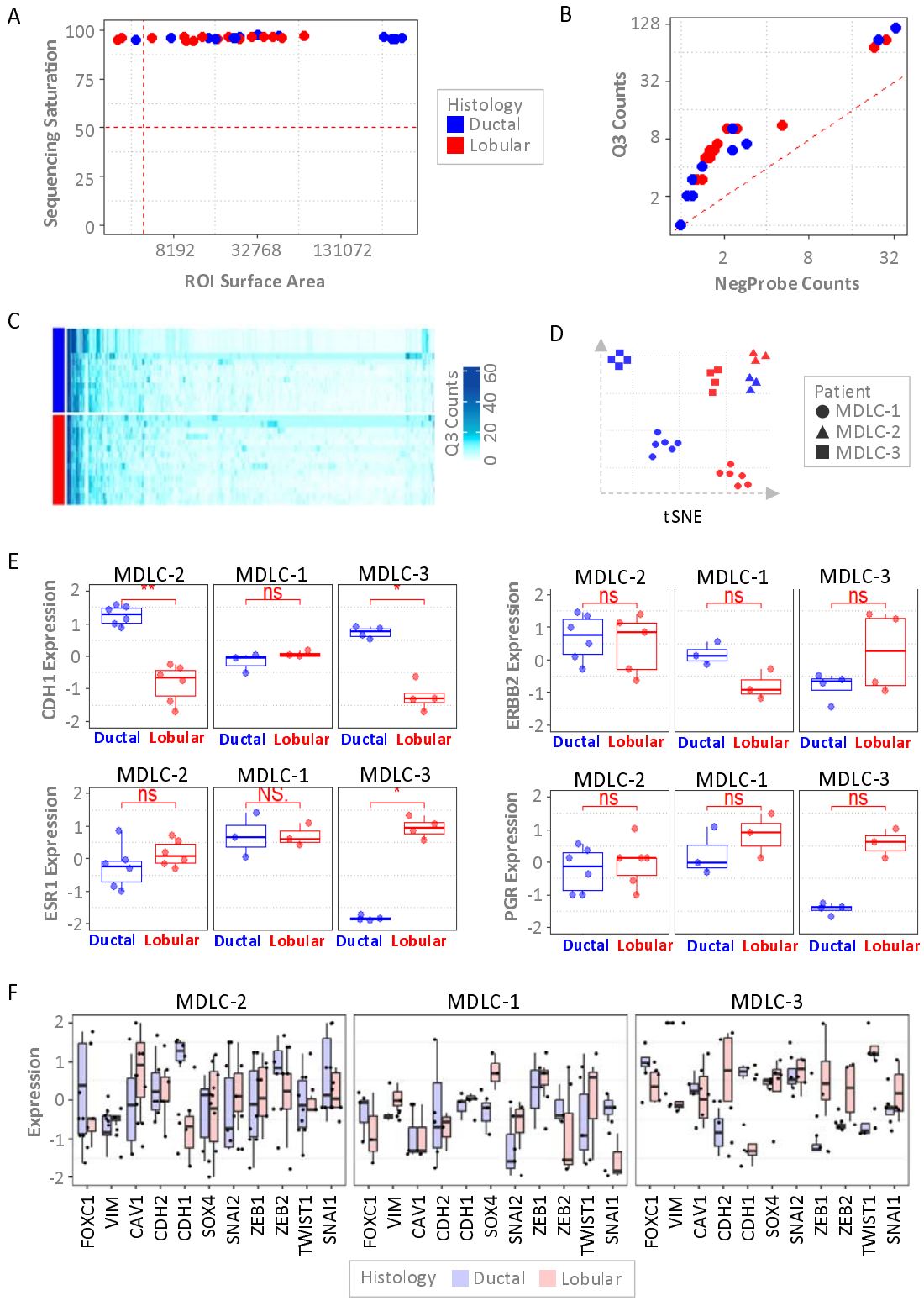


**Supplementary Figure S1: Digital Spatial Profiling RNAseq Dataset Quality Control.**

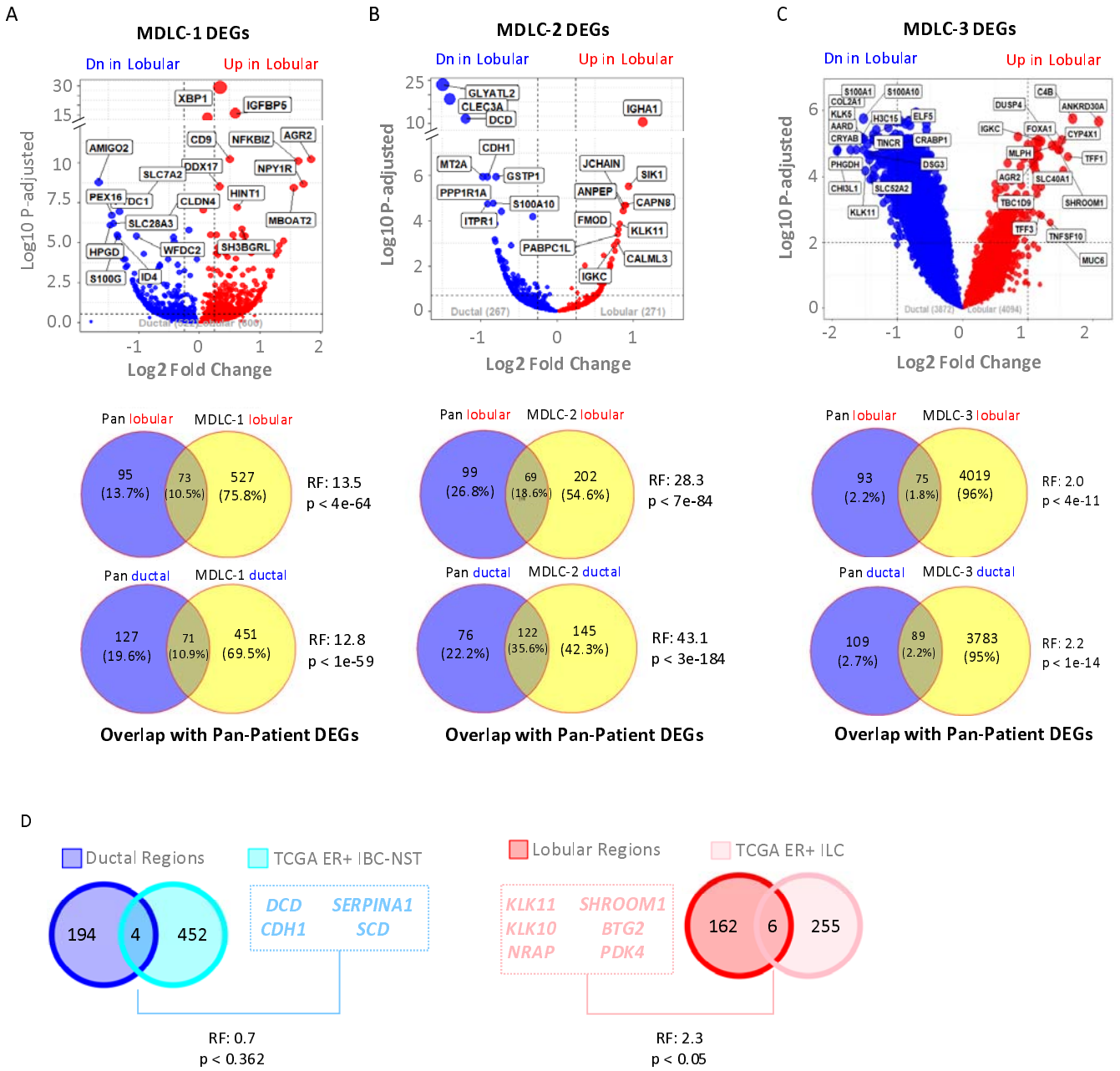


**Supplementary Figure S2: Patient Wise and Pan-Patient mDLC Ductal vs Lobular Differential Analysis.**

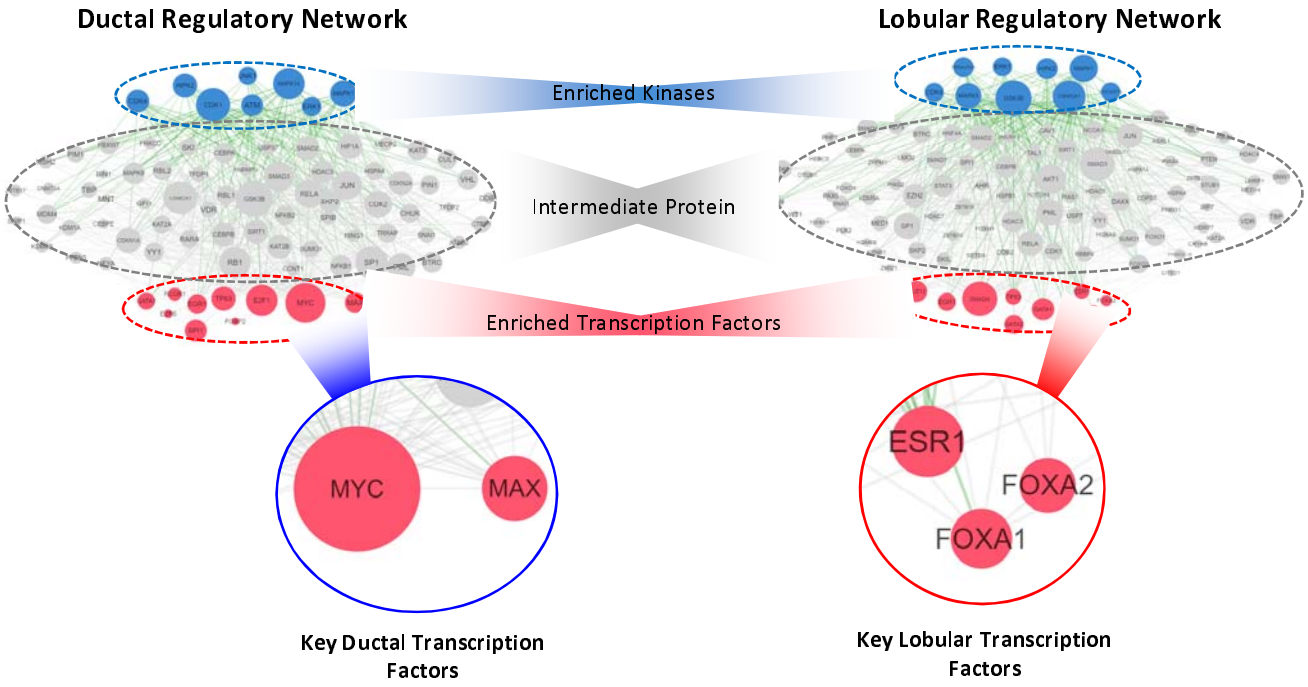


**Supplementary Figure S3: Transcription Factor Enrichment Analysis using Pan-Patient Ductal vs Lobular DEGs.**

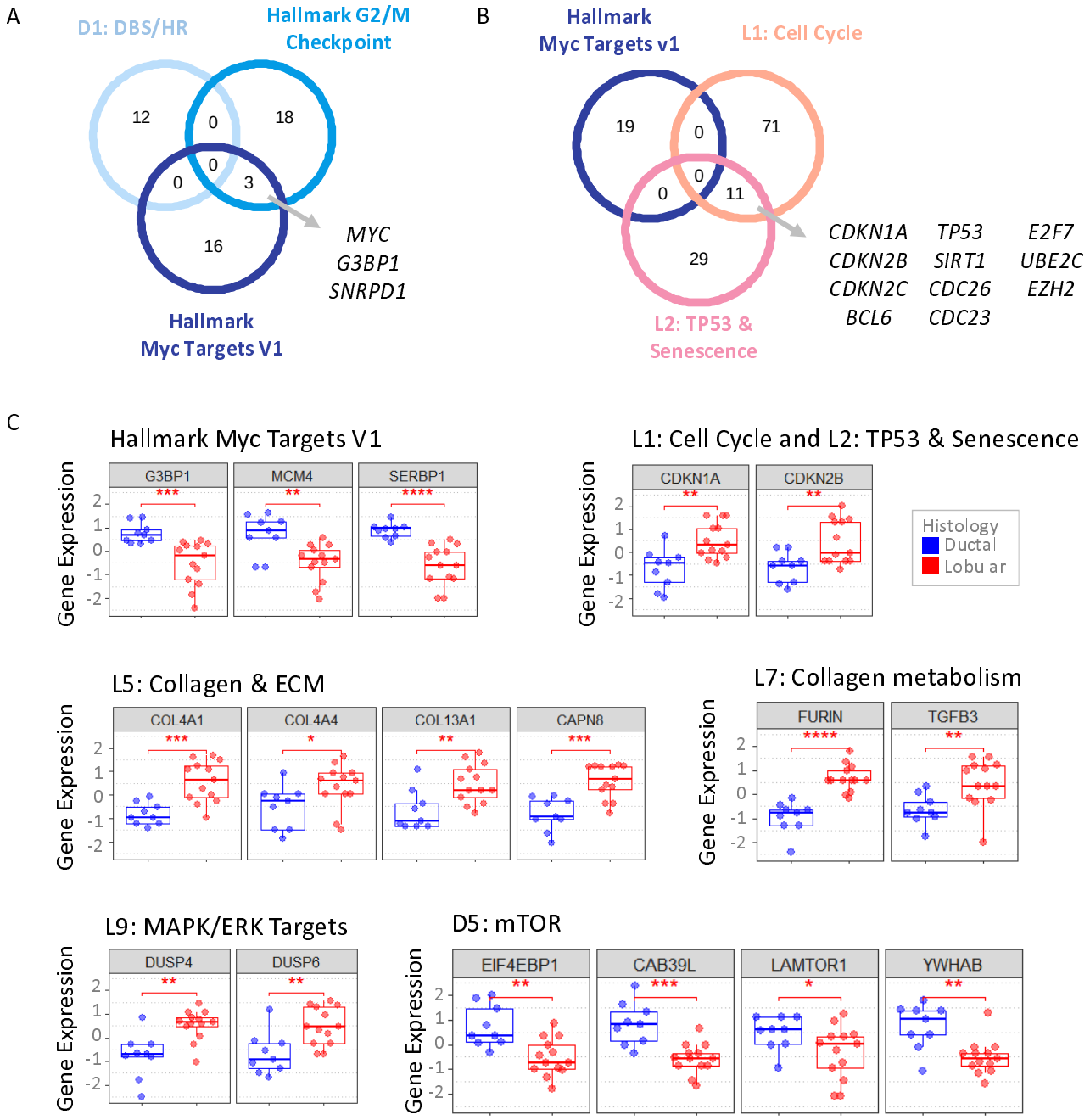


**Supplementary Figure S4: Key Genes Associated with Notable Differentially Enriched Oncogenic and Biological Signatures.**

A

| | Sample | Purity | Depth | Ploidy |
|---|---|---|---|---|
| MDLC-1 | Ductal | 0.36 | 428x | 2.02 |
| | Lobular | 0.45 | 523x | 1.97 |
| MDLC-2 | Ductal | 0.51 | 416x | 2.04 |
| | Lobular | 0.31 | 339x | 2.02 |
| MDLC-3 | Ductal | 0.62 | 378x | 3.35 |
| | Lobular | 0.4 | 490x | 2.01 |

C

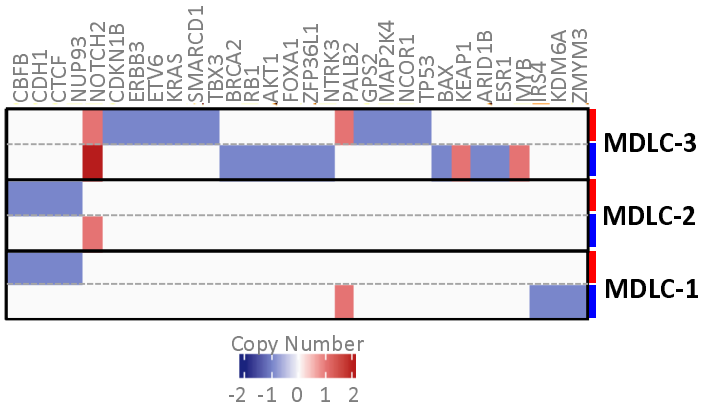


B

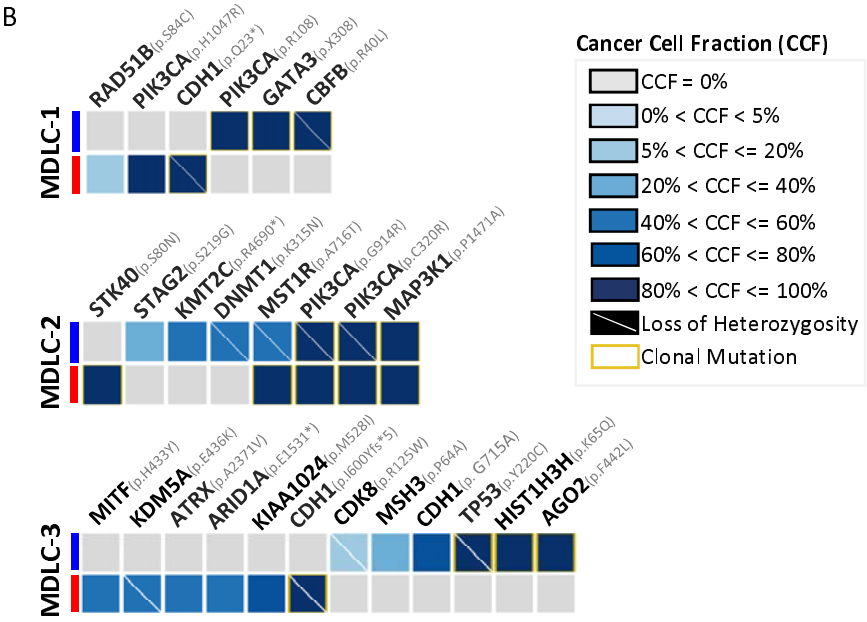


**Supplementary Figure S5: MSK-IMPACT Extended Results.**

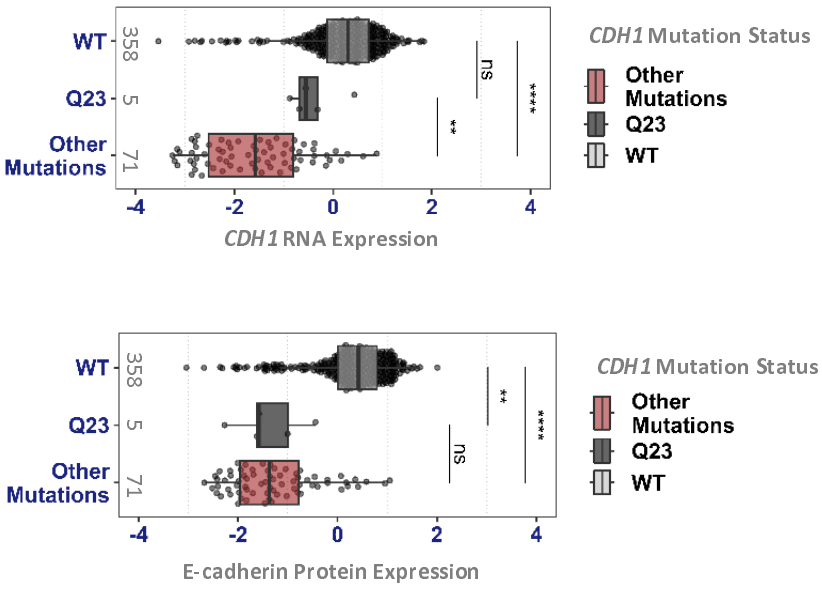


**Supplementary Figure S6: Effect of Q23 mutation on *CDH1* RNA and E-cadherin protein expression in ER+ Breast Tumors.**

A

| Metric | Value |
|---|---|
| Estimated Number of Cells | 4,671 |
| Fraction of Reads in Cells | 90.6% |
| Mean Reads per Cell | 91,174 |
| Median Genes per Cell | 1,481 |
| Total Genes Detected | 24,726 |
| Median UMI Counts per Cell | 4,480 |
| Number of reads | 425 million |
| Valid Barcodes | 96% |
| Sequencing Saturation | 78.4% |

B

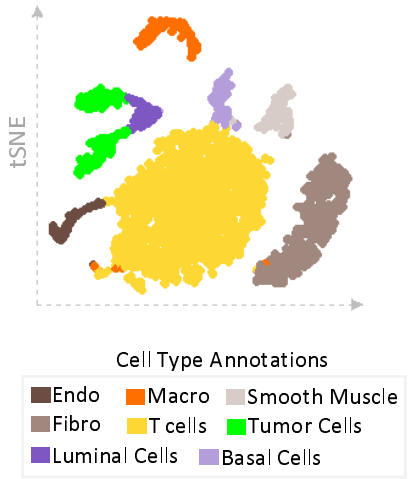


C

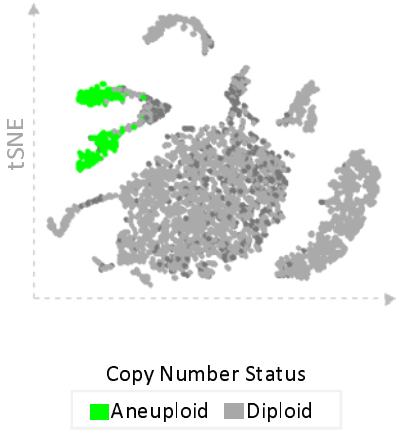


D

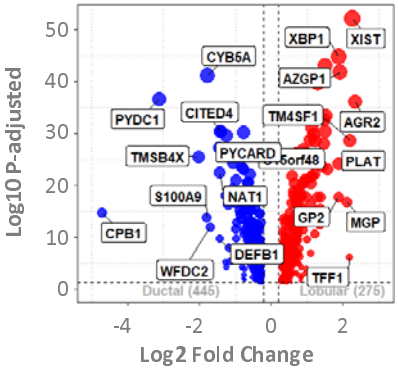


E

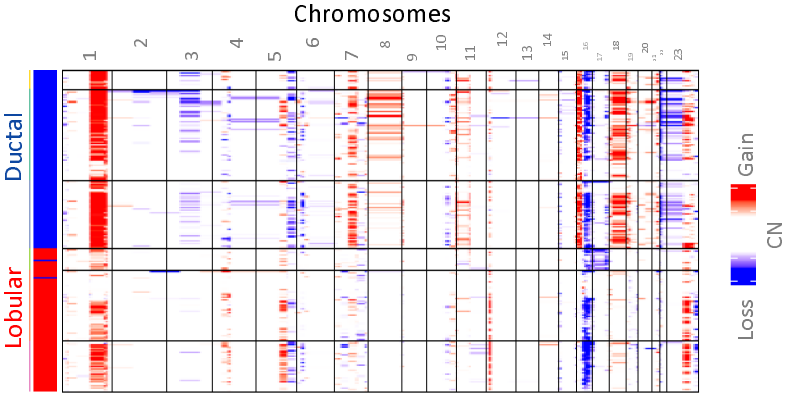


F

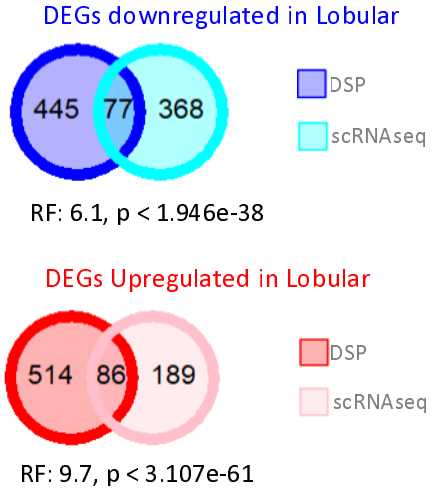


G

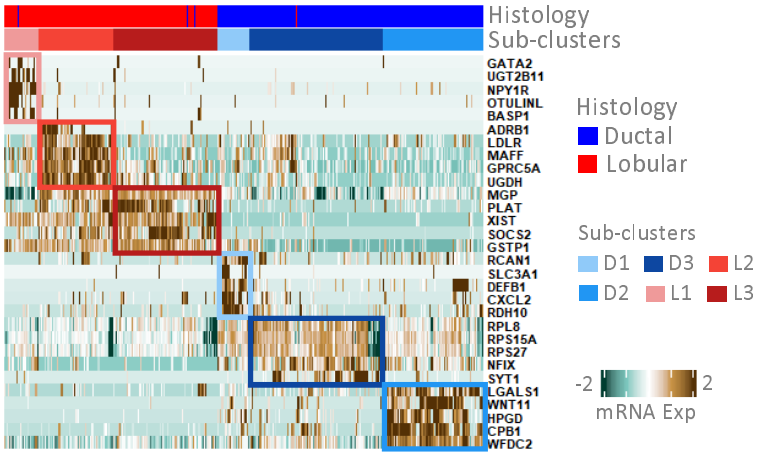


**Supplementary Figure S7: MDLC-1 Ductal and Lobular Tumor scRNAseq Heterogeneity.**

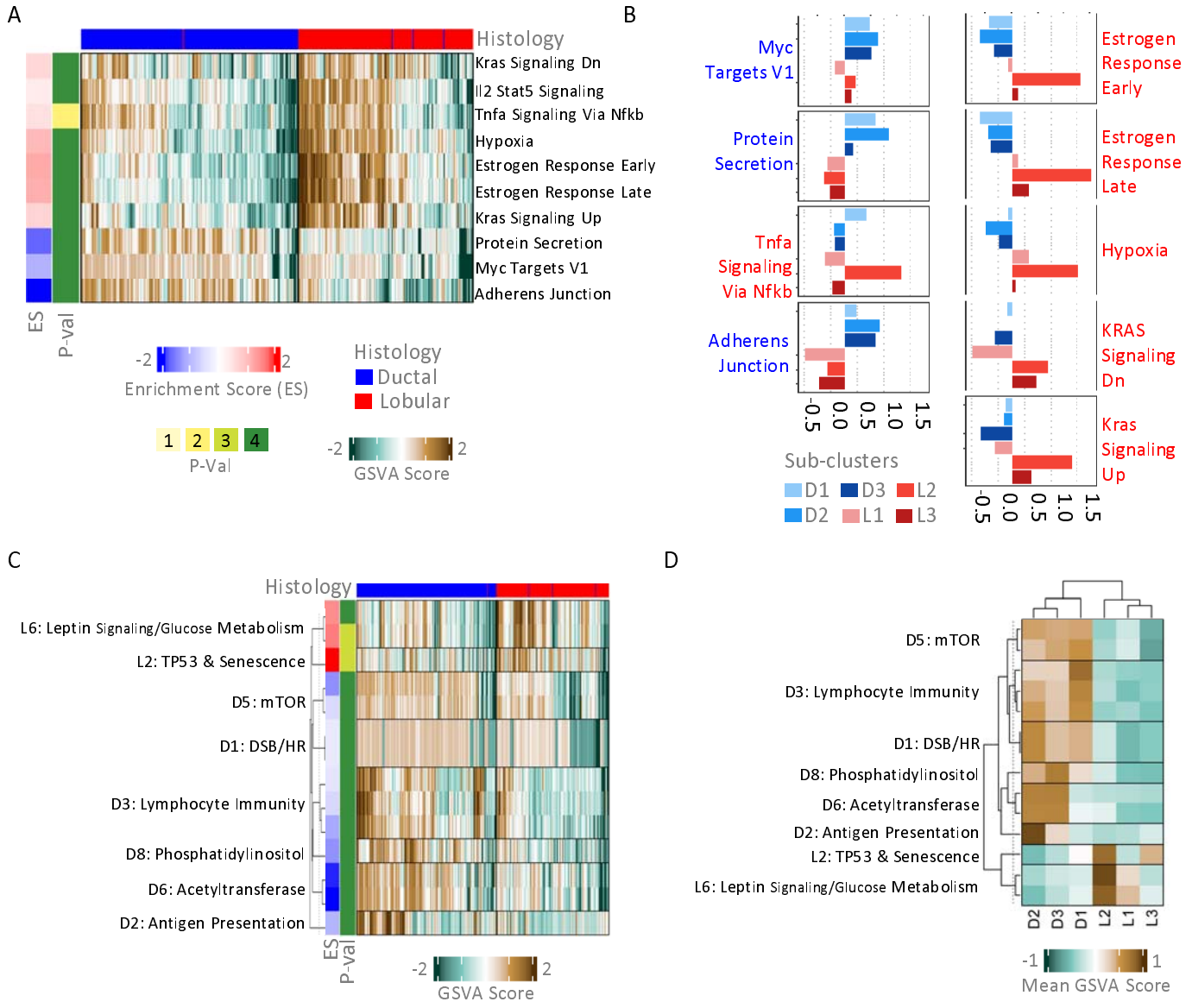


**Supplementary Figure S8: Distinct Biological Signatures in MDLC-1 Ductal and Lobular Tumor scRNAseq.**